Ore Geology Reviews 132 (2021) 104065

Contents lists available at ScienceDirect

Ore Geology Reviews

journal homepage: www.elsevier.com/locate/oregeorev

Cu-Au mineralization of the Sin Quyen deposit in north Vietnam: A product of Cenozoic left-lateral movement along the Red River shear zone

Van-Hao Duong [a], Phan Trong Trinh [b,c,d,*], Thanh-Duong Nguyen [a], Adam Piestrzyski [e], Dinh Chau Nguyen [e], Jadwiga Pieczonka [e], Xuan Dac Ngo [a], Phong Tran Van [b], Binh Thai Pham [f], Huong Nguyen-Van [g], Liem Ngo Van [g], Dieu Tien Bui [h], Dang Vu Khac [i], Chi Tien Bui [j]

[a] Hanoi University of Mining and Geology (HUMG), Hanoi, Viet Nam
[b] Institute of Geological Sciences, Vietnam Academy of Science and Technology, Hanoi, Viet Nam
[c] Graduate University of Science and Technology, Vietnam Academy of Science and Technology, Hanoi, Viet Nam
[d] Royal Academy for Overseas Sciences, Brussels, Belgium
[e] AGH University of Science and Technology (AGH-UST), Krakow, Poland
[f] University of Transport Technology, Hanoi 100000, Viet Nam
[g] VNU University of Science, Vietnam National University, Hanoi, Viet Nam
[h] GIS Group, University of South-Eastern Norway, Gullbringveggen 36, N-3800 Bø i Telemark, Norway
[i] Faculty of Geography, Hanoi National University of Education, Hanoi, Viet Nam
[j] Marine Geology and Minerals Division, Hanoi, Viet Nam

ARTICLE INFO

Keywords:
IOCG Sin Quyen deposit
Red River shear zone
Ore structure
U-Pb dating
Ar/Ar dating
Zipper tectonic model

ABSTRACT

The Sin Quyen iron oxide–copper–gold (IOCG) deposit is located in the southwestern part of the Sin Quyen Formation, close to the Red River shear zone. The deposit is controlled by the Sin Quyen fault, parallel to the Red River fault system in North Vietnam. U-Pb dating of zircon and uraninite and $^{39}Ar/^{40}Ar$ dating of biotite and K-feldspar in the Sin Quyen deposit showed that the mineralization was emplaced in two main phases: the first phase formed magnetite, uraninite, and allanite of Precambrian age, between 520 and 744 Ma; the second most important phase introduced Cu-sulfides with Au, this event formed chalcopyrite, pyrrhotite, and pyrite in the temperature range 320 ± 40 °C between 88 and 22 Ma. In this study, a tectonic model was presented to explain when and how the Sin Quyen IOCG deposit and some other Cu-Au deposits along the Ailao Shan Red River Shear zone occurred in Cenozoic time.

1. Introduction

Iron oxide–copper–gold deposits were studied by a number of authors, e.g (Hitzman et al., 1992; Sillitoe, 2003; Williams et al., 2005; Porter, 2010; Chen, 2013). IOCG deposits are known for comprising a broad spectrum of mineralization styles with hydrothermal Fe-oxides and Cu-sulfides as major components with low-Ti (Hitzman et al., 1992; Hitzman, 2000; Sillitoe, 2003; Williams et al., 2005). Besides the main mineralization, rare earth elements (REE), uranium, and precious metals could also be formed. One famous deposit is the Olympic Dam with the largest endowment of uranium in the world (Hitzman and Valenta, 2005; Skirrow, 2011), the second endowment of copper (Sillitoe, 2012) and significant gold (Kerrich et al., 2000; Frimmel, 2008; Porter, 2010).

The Sin Quyen is one of the largest IOCG deposit in the north of Vietnam (Pham et al., 2011; Zhao and Zhou, 2011; Tran et al., 2016). It is located in the Lao Cai province, in the Proterozoic metamorphic and sedimentary rocks of the Fanxipan uplift, and is restricted to its southwestern part, adjacent to the Red River shear zone (Fig. 1) (Leloup et al., 1995). The deposit is characterized by the unusual composition of its ore with pyrrhotite-chalcopyrite-gold-allanite-magnetite and uraninite (McLean, 2001; Pieczonka et al., 2015). The reserves of Cu, REE, S, Au

* Corresponding author at: Institute of Geological Sciences, Vietnam Academy of Science and Technology, Hanoi, Viet Nam.
E-mail addresses: haodnth@gmail.com (V.-H. Duong), phantrongt@yahoo.com (P.T. Trinh), nguyenthanhduong@humg.edu.vn (T.-D. Nguyen), piestrz@agh.edu.pl (A. Piestrzyski), nguyen.chau@fis.agh.edu.pl (D.C. Nguyen), jpieczon@agh.edu.pl (J. Pieczonka), dacbmks@gmail.com (X.D. Ngo), phongka160689@gmail.com (P. Tran Van), binhpt@utt.edu.vn (B. Thai Pham), huongtectonics@vnu.edu.vn (H. Nguyen-Van), liemnv@hus.edu.vn (L. Ngo Van), dieu.t.bui@usn.no (D. Tien Bui), dangvukhac@gmail.com (D. Vu Khac), buitien.dcksb@gmail.com (C.T. Bui).

https://doi.org/10.1016/j.oregeorev.2021.104065
Received 3 August 2020; Received in revised form 2 February 2021; Accepted 10 February 2021
Available online 18 February 2021
0169-1368/© 2021 Elsevier B.V. All rights reserved.

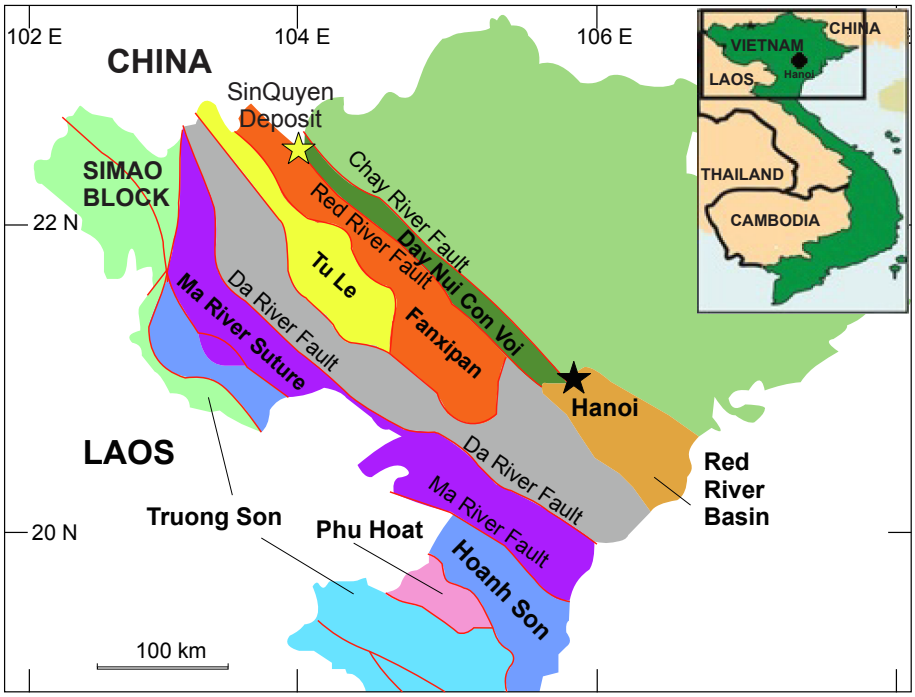


Fig.1. Main tectonic structures associated with the Sin Quyen Deposit *(modified from* Jacqueline et al., 2016*)*.

and Ag are 550,000, 334,000, 843,000, 34.7 and 25.3 tons, respectively (ESCAP, 1990). Recent exploration has reported over 100 million tons of copper ore (http://dongsinquyen.vn, 2013). Since 2006, the Sin Quyen deposit has been exploited as an open-pit mine with an annual average production of 12,000 tons of copper. One million tons of ore and six million cubic meters of host rocks are excavated annually (Le et al., 2015). In this study, the authors intend to present arguments on ore structures, temperature and the age of the Sin Quyen deposits, thereby relating these to the great role of the Cenozoic left-lateral motion along the Red River shear zone. A kinematic model termed "zipper tectonics" is proposed to explain when and how cooling and formation of the Sin Quyen deposit and other IOCG ores took place. In the zipper tectonic model, the clockwise rotation of the Indochina block produced three different zones of compressive, pure strike-slip, and extensional regimes.

2. Geological characteristics

2.1. Tectonic settings

The Red River shear zone is more than 1000 km long, forming the Ailao Shan–Red River metamorphic zone (ASRR) with Ailao Shan, Diancang Shan, Xuelong Shan in China, and Day Nui Con Voi in North Vietnam (Leloup et al., 1995). The metamorphic rocks distributed along the Red River shear zone consist of mylonitic gneiss. Foliation planes are steep and lineation is sub-horizontal, parallel to the elongation of the gneissic core (Leloup et al., 1995). The C–S structures, boudinage, rolling structures, and asymmetric quartz axis fabrics indicate that the gneisses have undergone left-lateral shear.

Heterogeneous deformation generates a composite fabric defined by foliation planes (S-surfaces) deflected into parallelism with narrow zones of concentrated shear parallel to the main shear zone. The C-shear bands also designated as C-surfaces. The C planes maintain a constant orientation, but the S planes rotate with increasing shear strain so that the angle between the two sets reduces to close parallelism in highly sheared mylonites. The S foliation is leaning over in the direction of shear and has an acute bulk inclination to the C-surfaces.

The length of the DNCV is approximately 300 km along the north bank of the Red River. In southern Yunnan, this fault splays into two parallel strands, which share a border with the DNCV to the north and south. In general, both fault-strands are Quaternary right-lateral slips (Trinh et al., 2012, 2013; Liem et al., 2016a). The Paleozoic granite massif in the Chay River zone was deformed in the Cenozoic (Roger et al., 2000; Krenn and Huong, 2019). Along the Bao Yen cross-section, the foliation planes are steep, dipping toward the south west or north east. The stretching lineation is sub-horizontal and clearly determined. U/Pb and $^{39}Ar/^{40}Ar$ dating revealed Eocene–Oligocene ages (Leloup et al., 1995, 2001).

Overthrusting was primarily observed in regions such as Sapa marble, Hoa Binh, and Phong Tho (Trinh et al., 1998). The left-lateral movement along the Red River shear zone continued after 19–17 Ma. A rest phase lasted from 12 to 5 Ma (Leloup et al., 1995; Huong et al., 2020). The Red River zone was active in the Quaternary and remains seismically active at the present time (Phuong et al., 2018; Truyen and Phuong, 2019; Duan and Duong, 2017; Nhung et al., 2017, 2018; Liem et al., 2016a; Thanh et al., 2018). Triassic limestone thrust on top of the Yen Chau strata was observed on the Moc Chau plateau (Findlay and Trinh, 1997; Trinh et al., 2013). The Song Chay River valley, which can be clearly seen on Landsat and SPOT images, is located in the northeast of DNCV (Liem et al., 2016b).

The Sin Quyen deposit is located in the northeastern part of the Fanxipan zone, stretching for 300 km in a northwest direction. The Fanxipan zone, dominated by Proterozoic rocks, is a fragment of the Yangtze Platform in south China (Leloup et al., 1995; McLean, 2001; Nguyen et al., 2019). The deposit occurs within the Red River metamorphic belt (Hsin et al., 2013; Tapponnier et al., 1990). The rocks from this zone have been dated to 2360–1960 Ma (Tran, 2001), 1700–1659 Ma (Zhao and Zhou, 2011; Bui et al., 2004), early 575–430 Ma and later reactivated at 82–22 Ma *(this study),* 263–240 Ma (Zelazniewicz et al., 2013), 40–22 Ma (Leloup et al., 1995; Anczkiewicz et al., 2000, 2007; Lepvrier et al., 2008; Trinh et al., 2013; Thao et al., 2017; Tran et al., 2014a, 2014b; Liu et al., 2015), with the youngest events occurring at 34–5 Ma, and 17–5 Ma (Nguyen et al., 2013). In the northeastern part of the deposit, the DNCV metamorphic complex (263–240 Ma Zelazniewicz et al., 2013) is situated in the southwest of the Da River belt (McLean, 2001) (Fig. 1), which is the boundary between South China and Indochina blocks in northern Vietnam (Jacqueline et al., 2016).

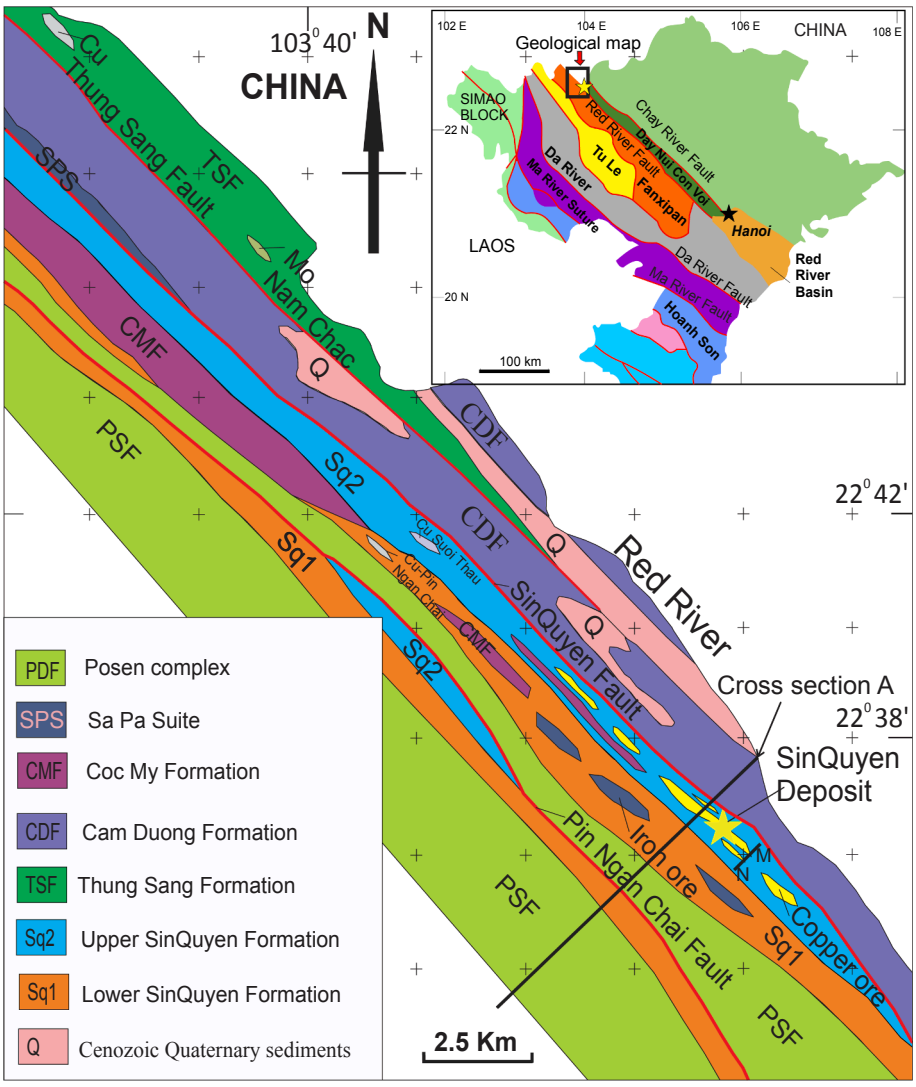


Fig. 2. The geological map of the region (Yellow star symbol indicates center of the copper deposits) (modified from Van et al., 2021).

Between South China and Indochina, there are a few major northwest-southeast trending faults: the ASRR fault system including the Chay River fault (Gilley et al., 2003) and the Red River, the Da River, and the Ma River faults (Kazuhiro et al., 2005; Tran and Hoang, 2018).

The southwest part of the Red River fault consists of five northwest - southeast oriented main structural units (Tran, 1979) from east to west: the 250 ± 3 Ma Fanxipan crystalline massif (Pham et al., 2013; Hieu et al., 2013; Usuki et al., 2015); the 256 ± 4 Ma Tu Le continental rift system (Tong-Dzuy and Vu, 2011), containing volcaniclastic formations; the 263 ± 7 Ma Da River rift zone (Balykin et al., 2010), comprising a diversity of marine volcanic and sedimentary sequences inverted in the Jurassic (Le and Ngo, 1995; McLean, 2001); the 243 ± 13 Ma Ma River structure (Pham et al., 2008; Zhang et al., 2013) composed of greenschist facies oceanic sediments and volcanics in ophiolites along the Ma River Fault (Metcalfe, 1995; McLean, 2001) and the Truong Son Fold Belt. The Da River Belt and the Dien Bien Phu fault are located in the northwest. This zone is a strike extension of the Pak Lay fold belt in Laos, which formed during the Late Jurassic collision of the Shan Thai and Indochina blocks. Various formation ages show that Sin Quyen deposit is located within a tectonic zone that was reactivated many times.

2.2. Stratigraphy

The Sin Quyen deposit occurs within the Proterozoic Sin Quyen formation (Fig. 2). The Sin Quyen formation includes sedimentary and metamorphic sediments containing copper bodies in contact with Cambrian Paleozoic sediments of the Cam Duong formation and a small element of Quaternary sediments. They are to a large extent controlled by the Sin Quyen reverse fault and a number of regional dislocations, including the Sin Quyen, Pin Ngan Chai, and Thung Sang faults. All of them are parallel to the major Red River Fault (RRF) (Ta et al., 1975; McLean, 2001; Nguyen et al., 2017).

The Sin Quyen formation is situated within highly deformed amphibolites, migmatised gneisses and schist, extending along a northwest - southeast strike, dipping 50–85°, and with an average width of 400–800 m (Ta et al., 1975; McLean, 2001; Gaskov et al., 2012. From the facies point of view, this is divided into upper and lower Sin Quyen formation units.

The upper Sin Quyen formation is in tectonic contact with the Cam Duong formation and the Cambrian Sa Pa Suite (McLean, 2001), composed of limestone. The lower Sin Quyen formation is underlain conformably by Proterozoic *meta*-sediments of Lung Po formation (McLean, 2001; Ishihara et al., 2011).

The upper Sin Quyen formation is the main bedrock located in the northeastern part of the deposit, composed predominantly of plagioclase [61%], quartz [21%], biotite [15%] and with accessory apatite, sphene, calcite, and garnet (Ta et al., 1975; McLean, 2001). The mineral compositions of the lower Sin Quyen formation are quartz [50%], graphite

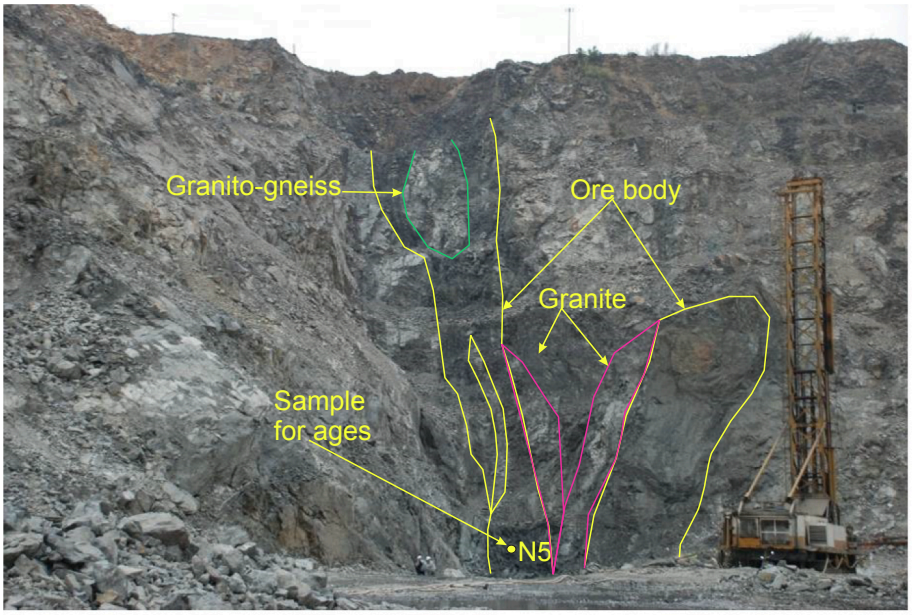


Fig. 3. Satellite image and sampling points for the IOCG Sin Quyen deposit.

[15%], biotite [10%] and muscovite [12%], with plagioclase, tourmaline, garnet and sillimanite as the minor.

The upper Sin Quyen formation is strongly crushed and metamorphosed, which makes it more complex with multiple layers of schist, and it is migmatized. The host rocks are amphibolite, granite-gneiss, with some contact with granite and other altered rocks (Ta et al., 1975; McLean, 2001).

The Cam Duong formation located in the northeast of the deposit, extending along the northwest - southeast strike, dip at 20–70^0. The rocks include quartz-sericite schist, containing coal, schist-quartz, quartz-biotite–chlorite schist, plagioclase, and apatite (Ta et al., 1975).

Quaternary sediments near the Sin Quyen copper deposit are very thin, including pebble, sand, clay, and sandstone sourced from weathered Po Sen granitoid, granosyenite, granito gneiss, gneiss, and crystalline schist (Ta et al., 1975).

2.3. Magmatism

The magmatic rock is divided into Proterozoic Coc My formations (including amphibolite and granite-gneiss) and Permian assemblages (including gabbro–dolerite and plagiogranite) (McLean, 2001; Ta et al., 1975).

Amphibolite bodies occur in the Sin Quyen formation with a thickness ranging from 5 to 50 m and 10 m to 100 m in length, along a northwest - southeast strike, with variable geometries, a well-defined foliation and often a banded texture (McLean., 2001; Ta et al., 1975). The rock comprises hornblende [66%], plagioclase [19%], biotite [6%] and minor orthite, epidote, apatite, chlorite, calcite and ore minerals (McLean, 2001; Ta et al., 1975; Ishihara et al., 2011). Plagioclases are commonly sericiticized (McLean, 2001). Close to the ore bodies or in the altered zone, there are additional minerals like allanite, calcite, and sulfide minerals vein (Ta et al., 1975). The altered amphibolite intervals host approximately 70% of the ore mineralization in the deposit and all of the higher-grade zones. This section is represented by disseminated pyrrhotite, pyrite, and minor chalcopyrite.

Highly-deformed and migmatised granite-gneiss represented as lenses with thickness ranging from 2 to 200 m, 10–3000 m in length, and extending along the northwest-southeast strike. The rock comprises plagioclase [66%], quartz [26%], biotite [7%], while zircon and apatite are minor elements (Ta et al., 1975). The plagioclases among them are microlined and sericiticized, while the quartz is crushed and biotite is sheared.

Gabbro–dolerite occurs between the Sin Quyen formation and the Sa Pa suite, extending the northwest - southeast strike (McLean, 2001; Ta et al., 1975). Its mineral compositions are amphibole [64%], plagioclase [18%], biotite [7%], chlorite [5%], calcite and disseminated pyrite, pyrrhotite and chalcopyrite (McLean, 2001; Ta et al., 1975; Ishihara et al., 2011).

The plagiogranite occurs in fracture zones of the deposit, 1–20 m in thickness, 10–300 m in length, which is related to the fracture zone cross-cutting all of the Sin Quyen formation, Sa Pa suite and Coc My formation along the faults. The major components are plagioclase [63%], quartz [26%], biotite [6%], microcline, muscovite, apatite, chlorite, sometimes zircon, and albite (Ta et al., 1975).

2.4. Metamorphism

The detailed study of the Red River shear zone indicated that the gneiss cores are composed of strongly foliated and lineated mylonitic gneisses. The foliation is usually steep, and the lineation nearly horizontal, both being parallel to the local trend of the gneissic cores (Leloup et al., 1995). Numerous shear criteria, rolling structures, asymmetric foliation boudinage and asymmetric quartz axis fabrics indicate that the gneisses have undergone intense, progressive left-lateral shear. P–T studies show that left-lateral strain occurred under amphibolite-facies conditions (3–7 kb and 550–780 °C) (Leloup et al., 1995). In both ranges, high-temperature shear was coeval with emplacement of leucocratic melts. The similarity of deformational kinematics, P–T conditions and crystallization ages in the Ailao and Diancang Shan metamorphic cores indicates that they represent two segments of the same Tertiary shear zone. Additional field evidence suggests that the Xuelong Shan zone in northern Yunnan and the Day Nui Con Voi zone in Vietnam are the respective northward and southward extensions of the ASRR shear zone. Garnet–sillimanite–plagioclase–quartz thermobarometry and garnet–biotite yielded the conclusion that left-lateral motion occurred in the DNCV with a high geothermal gradient, from amphibolite facies (3–7 kb and 550–780 °C) to greenschist facies (3.8 kb and 500 °C) (Leloup et al., 1995, 2001).

The metamorphic rocks are the principal hosts of the copper ore, with most of them localized in the central part of the deposit. They are mainly composed of pyroxene, garnet, hastingsite, quartz, albite, allanite, apatite, biotite, plagioclase, chlorite, epidote, and calcite.

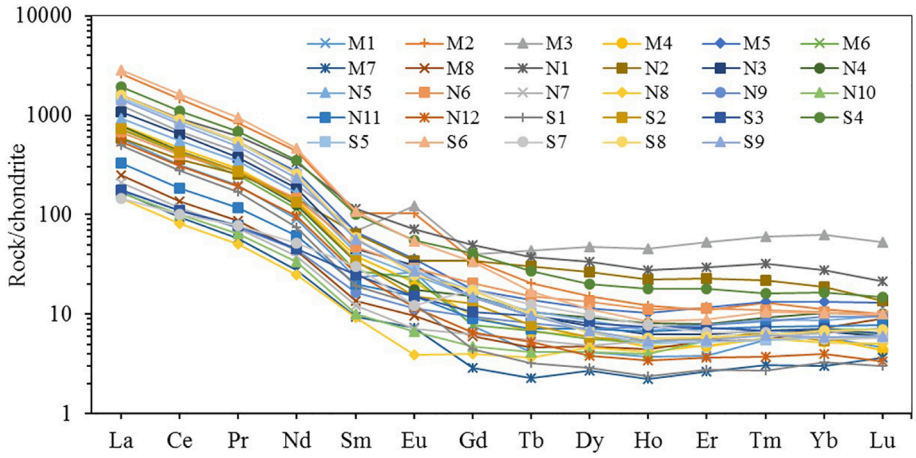


Fig. 4. Chondrite-normalized REE patterns for samples from the Sin Quyen deposit.

Metamorphosed rocks are divided into two groups: the skarn-pyroxene-garnet group with pyrrhotite ores, and rare prevalence of chalcopyrite; and the skarn-hastingsite-biotite-quartz group, including magnetite ore, uraninite, sulfide ore (mainly chalcopyrite-pyrrhotite) replacements and fill cracks. In some places, they are cut by altered dykes, in which quartz veins with copper mineralization are observed. There are greatly differing forms of altered rock occurring, they can be a series of lenses, chambers or vein bunches of 0.5 to 100 m in thickness and 1 to 1000 m in length, trending along the northwest - southeast strike and dipping 65−90° (Ta et al., 1975).

3. Field work and analytical results

3.1. Field works

Geological field surveys and sample collecting were performed as part of an international project supported by Grant No 01/2012/HD-HTQTSP. The field geological surveys and sample collecting were

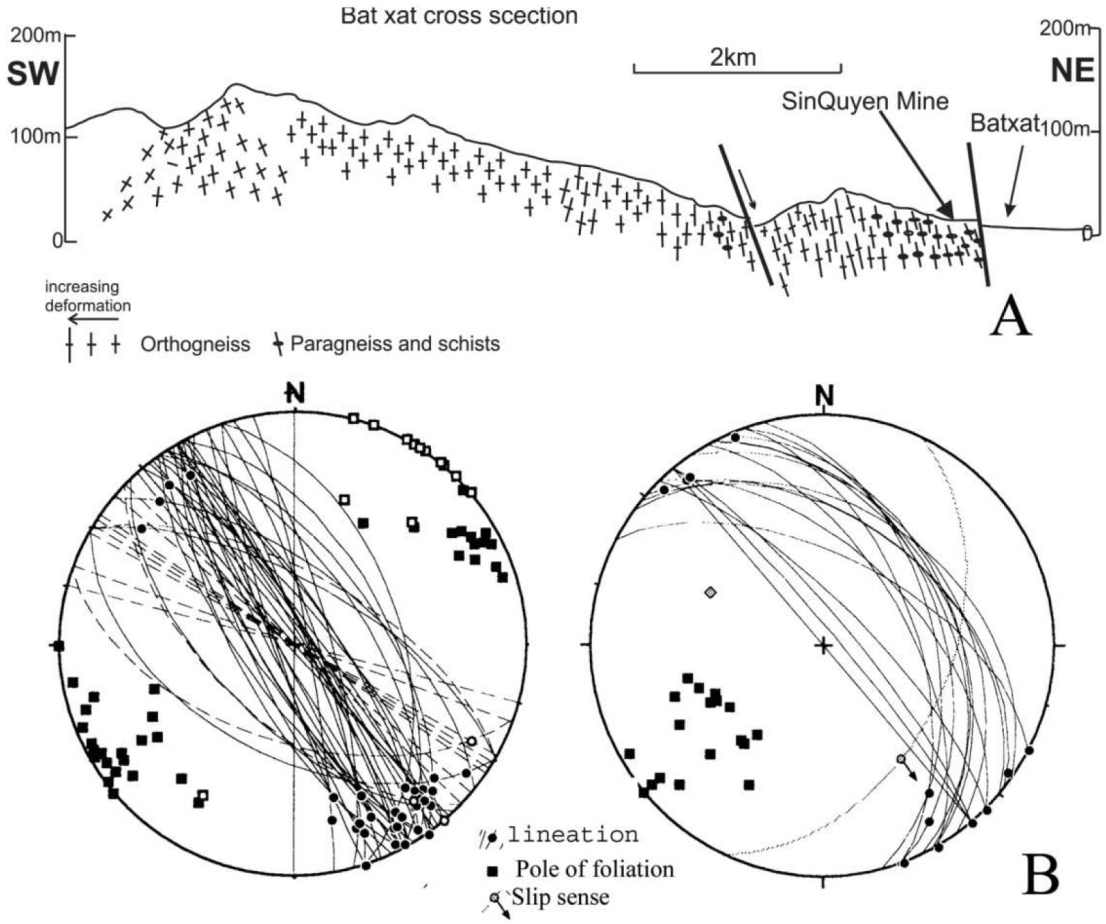


Fig. 5. a. A cross-section with the location of the Sin Quyen Mine. Foliation planes are almost sub-vertical, and striation is almost sub-horizontal. Various shear critera indicate left-lateral movement along the NW-SE direction (modified from Leloup et al., 2001). b. Structural diagram of sub-vertical foliation planes at the Bat Xat and Sin Quyen Mine (modified from Leloup et al., 2001).

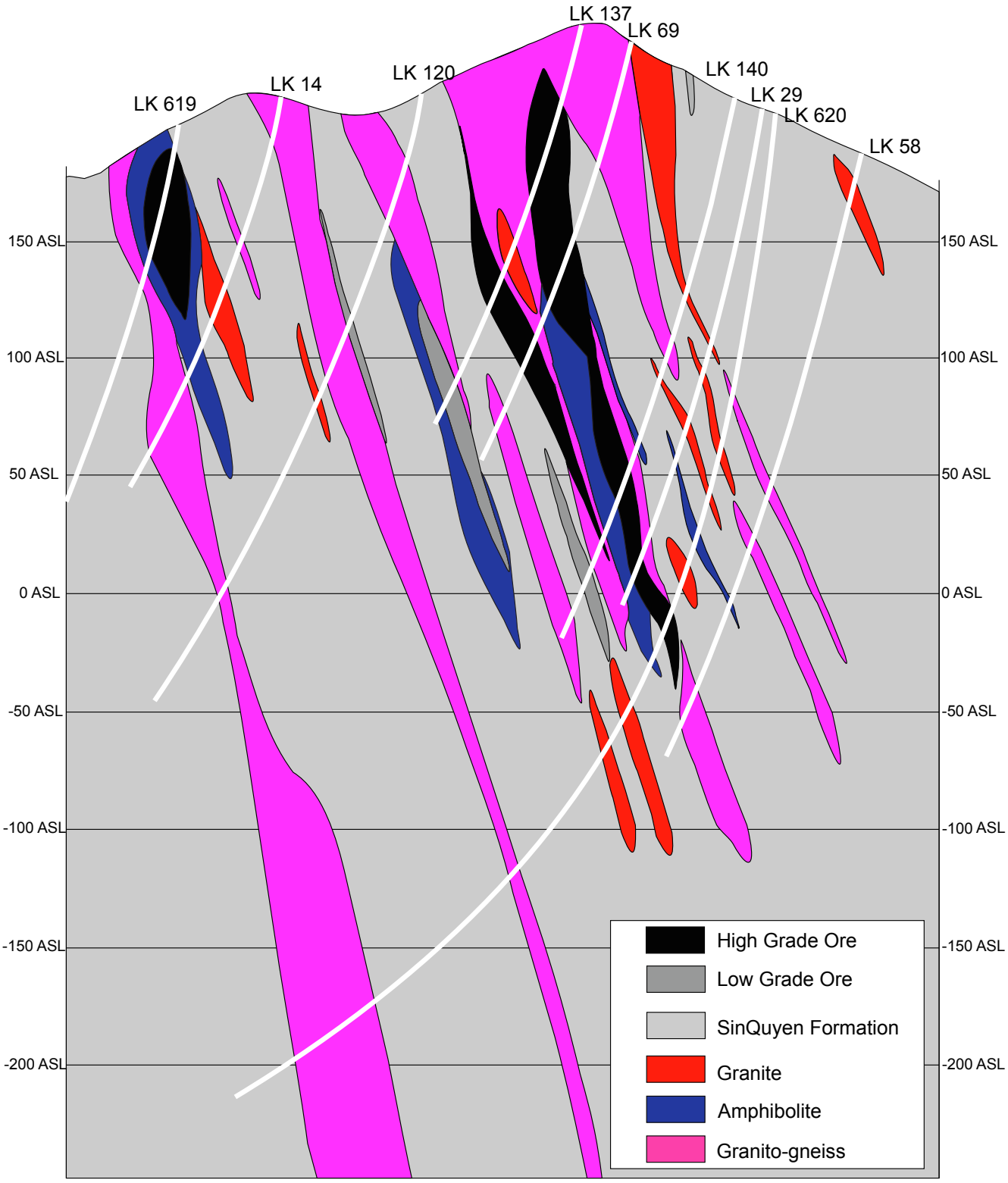


Fig. 6. Ore structure of the Sin Quyen deposit. From left to right corresponding the northeast-southwest profile of the Sin Quyen deposit. Ore bodies coincide with foliation planes. The amphibolite boudinage and ore structure are compatible with left lateral movement of the Red River Shear Zone (modified from Ta et al., 1975).

divided and conducted during two periods. First, the geological survey was performed both inside and outside of the Sin Quyen deposit. This work was carried out simultaneously with sampling and ground gamma spectrometric measurements for all kinds of recognized rocks and ore. In total, 44 samples were collected, and 44 gamma spectrometry points were measured. 29 rock and ore samples were collected in the principal orebody and perpendicular strike of the ore body. Fig. 3 shows the sampling points. All the collected samples were sent to laboratories at AGH UST Kraków, Poland and ACME Bureau Veritas Commodities in Canada for further analysis.

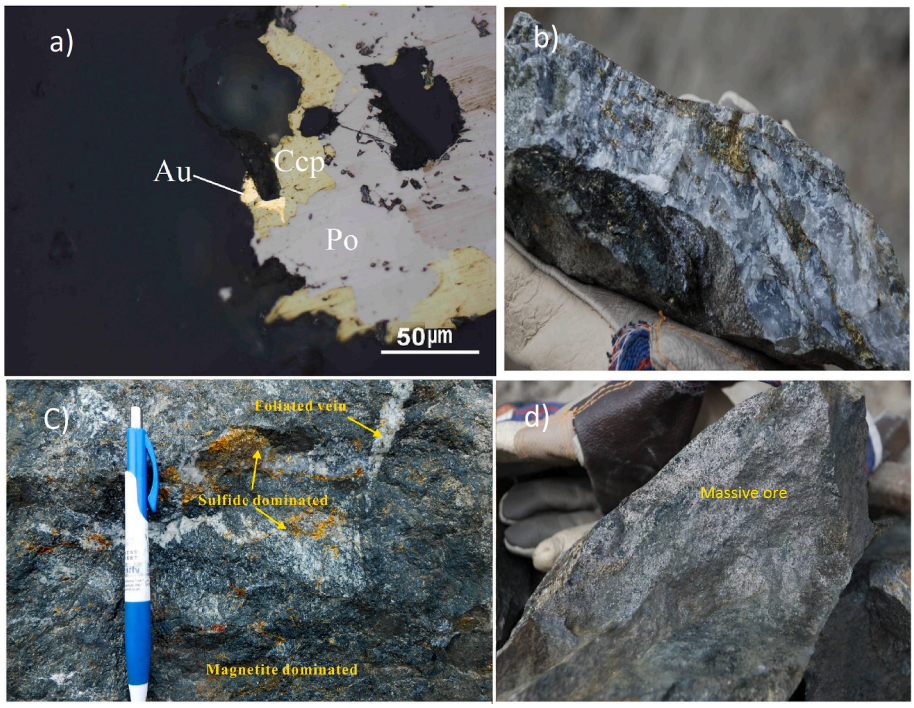


Fig. 7. a. Gold (Au) in chalcopyrite (Ccp) and pyrrhotite (Po) in reflected light; b. Quartz and sulfide veins; c. sulfide-dominated foliated and magnetite-dominated veins; d. massive ore.

3.2. Electron microscope analysis

Polished sections were prepared in the Polishing Laboratory of the Faculty of Geology, Geophysics and Environmental Protection (FGGEP), AGH UST, Poland. Then, the samples were investigated in reflected light using a Nikon Optihop polarizing microscope. The photographs were made with a Sony Exwave HAD digital camera integrated with a Nikon Optihop ore microscope.

3.3. Uranium and REE analyses with Wavelength-Dispersive X-Ray Spectroscopy (WDS)

Quantitative analyses were conducted in the Critical Elements Lab. of AGH-UST Krakow using JEOL SQ8200 microprobe. The following standards and measurement lines have been used: SiKα (albite), AlKα (kyanite), SKα (anhydrite), UMβ (UO2), YLα (YPO4), PKα(YPO4), ScKα (100%), TiKα (rutile), CeLα (CePO4), LaLα (LaPO4), ThMα (ThO2), CaKα (wollastonite), PrLβ (PrPO4), TbLα (TbPO4), DyLα (DyPO4), ErLα (DyPO4), LuLα (LuPO4), GdLβ (GdPO4), PbMα (crocoite), NdLα (NdPO4), SmLα (SmPO4), EuLβ (EuPO4), TmLα (TmPO4), YbLα (YbPO4), HoLβ (HoPO4), AsLα (InAs). Overlap correction of Nd-Ce, Sm-Ce, Lu-Dy, Dy-Eu, U-Th, Tm-Sm, Gd-Ho have also been implemented. Using the data on U, Th and Pb determined by WDS, the absolute age of uraninites has been estimated. For uranium dating and decrease of the detection limit, the following peak/background conditions (in sec.) were used. The U, Th, and Pb in uraninite were analyzed by WDS measurements using an electron microprobe with the accelerating voltage 15 kV, probe current 40nA, focused electron beam diameter 3 μm; counting times peak/background: U 120/60, Pb 180/90 and Th 120/60. Monazite crystal TS-Mnz (894.8 ± 5.3 Ma) was used as reference material for microprobe standardization.

3.4. Bulk and trace elements

Bulk chemical analyses of the ores and rocks were carried out by the Aqua Regia digestion method with Ultratrace ICP-MS analysis at ACME Labs - Bureau Veritas Commodities Ltd, Canada. The results for samples in the Sin Quyen deposit were presented through chondrite-normalized REE patterns.

The concentrations of the metallic elements and REE were analyzed in selected samples, collected from the ore, rock, concentrate and waste. The detailed results were presented in a Ph. D. thesis (Hao, 2018).

In the chondrite-normalized REE diagram (Fig. 4), all samples are enriched in the light rare earth elements (LREE). The light elements of the REE group dominate in the deposit.

4. Results

4.1. Ore structure and feature of minerals

In our field observations, the rocks in this area are dissected by the Sin Quyen, Pin Ngan Chai, and Thung Sang faults (Fig. 2). The mineralization in the Sin Quyen formation, which is divided into two units (upper and lower Sin Quyen formations): the upper is in tectonic contact with Cam Duong formation, the lower Sa Pa suite at depth; the lower is underlined conformably by Lung Po formation. The Sin Quyen deposit is covered within Quaternary sediments.

The ore bodies are hosted in altered amphibolite and migmatitic granite-gneiss within the metamorphosed sediments of the Sin Quyen formation. Ore bodies are steeply dipping, with lenses and elongate in shape, 100–200 m in thickness and approximately 2.5 km in length, trending along the northwest-southeast strike (Figs. 5 and 6).

There are four zones with three fracture systems. All zones are intensely deformed, and the rocks are strongly fractured and dislocated. The high-grade ore bodies are hosted in the largest zone (Fig. 6). There are three fracture systems: northwest-southeast, northeast-southwest, and northeast (Ta et al., 1975). All the fracture systems were developed before ore mineralization, and the northwest-southeast system is the youngest. Another fracture system was created after mineralization but did not have any impact on the ore position. There is also a fracture system with a northeast trend and almost vertical dip. It is well developed regionally and controls the secondary drainage (Ngoi Phat stream), which intersects the Sin Quyen deposit.

There are massive, disseminated, banded and/or stockwork-like

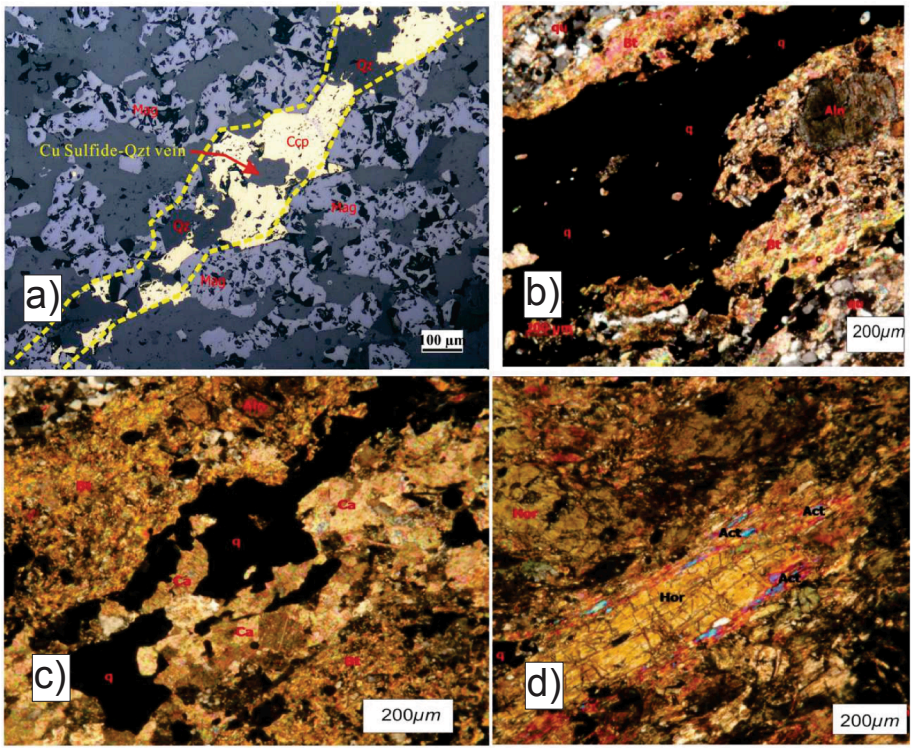


Fig. 8. a. Chalcopyrite (Ccp), magnetite (Mag) and quartzite (Qz) in reflected light. b. Biotite (Bt), allanite (Al), quartzite (Qu) and ore minerals (q). c. Biotite (Bt), allanite (Al), canxite (Ca), and ore minerals (q), d. Skarn hornblende (Hbl), actinolite (Act), and ore minerals (q).

structures of ore (Ta et al., 1975; McLean, 2001; Gaskov et al., 2012; Li and Zhou, 2018; Liu and Chen, 2019) (Figs. 7b-d, 8a). They could be divided into sulfide, oxide, and mixed oxide-sulfide ores, based on the relevant contents of Fe-oxide and Cu-sulfides. Based on the distribution of major minerals, the deposit was divided into eastern and western parts. The pyrite, pyrrhotite, and chalcopyrite are dominate in the eastern part, comprising nearly 90% of the ore. In the western part, chalcopyrite and magnetite prevail, and they constitute about 50% of the ore (Gaskov et al., 2012). These minerals often occur in the skarn zone together with copper and iron sulfides. The types of mineralization include: i) massive copper ore, ii) massive iron ore, iii) mixed Fe-Cu ores, iv) dispersion and v) vein types of ores. All ore types are characterized by different mineral assemblages (Figs. 9a-f, 7b-d, 8a). The main ore minerals are magnetite, pyrite, pyrrhotite, chalcopyrite, allanite and some ilmenite, marcasite, sphalerite, tennantite, cubanite, arsenopyrite, galena, Bi-native, bismuthinite, electrum, native gold, galena, and tellurobismuthite (Pieczonka et al., 2015, 2019).

The massive iron ore is composed of magnetite, allanite, pyrrhotite and minor amounts of pyrite, chalcopyrite and cubanite, with traces of uraninites. The mixed Fe-Cu ores consist of both assemblages mentioned above.

The magnetite, allanite, chalcopyrite and uraninite intergrowths occurred along with the fractures (Fig. 9a, c). The intergrowth with relevant mineralization was studied by Pieczonka et al. (2015), Pieczonka et al. (2019). They formed disseminations, veins and bands along foliations and massive accumulations, mainly in metasomatic rocks, but also the granite-gneiss adjacent and as grains on the margins of biotite and hastingsite (amphibolite) (McLean, 2001; Ishihara et al., 2011).

The 85% content of allanite has been reported in hastingsite-biotite-quartz metasomatites and up to 10% in the skarn type of rocks (McLean, 2001). This mineral appears in all types of ores in different quantities. In some ore sections studied under the microscope, allanite occupied up to 100% of the sample surface (with several square millimeters). Allanites usually form intergrowths with magnetite, amphibole, titanite, biotite, and sulfides. Besides, some inclusions of magnetite, carbonate, and sulfides are observed in grains of allanite (Pieczonka et al., 2015, 2019).

Uraninite formed crystals up to 150 µm in size and occur as intergrowths in the massive magnetite-sulfide-allanite ores, showing the same systems of cracks that implied simultaneous crystallization with magnetite and recrystallization of host rocks (Pieczonka et al., 2019). Some euhedral uraninite crystals, mostly biotite have been found in the magnetite and silicate matrix, mostly biotite. Under magnification, uraninites show a lack of homogeneity in color and a small difference in reflectivity and internal reflections (Pieczonka et al., 2015).

Gold occurs in pyrite and younger chalcopyrite within massive ores (Fig. 7a) or as free grains and as electrum (later, hydrothermal stage) (Pieczonka et al., 2015, 2019).

Some samples show the intergrowth of young chalcopyrite and quartzite veins, which fill in fractures of magnetite minerals, and ore minerals which fill fractures in quartz and calcite, and skarn hornblende (Fig. 8a-d).

4.2. U-Pb dating

Zircon mineral was checked by transmitted and reflected light with cathode-luminescence images to show their internal structures. U-Pb dating was carried out by laser ablation (LA)-inductively coupled plasma (ICP)-mass spectrometry (MS) at Wuhan, China. These instruments and the data reduction were described in Zong et al. (2017). A GeolasPro-COMPexPro 102 ArF excimer laser (wavelength 193 nm; maximum energy: 200 mJ) and a MicroLas optical system were employed for laser sampling. Ion-signal intensities were acquired using an Agilent 7700e ICP-MS instrument. Helium was used as a carrier gas, and argon was the make-up gas and was mixed with the carrier gas via a T-connector before entering the ICP. The laser ablation system includes a "wire" signal smoothing device (Hu et al., 2015). In this study, the spot size and frequency of the laser were fixed at 32 µm and 6 Hz, respectively. Zircon 91,500 and glass NIST610 were employed as external standards for U-Pb dating. Each analysis combined a background acquisition of approximately 20–30 s followed by 50 s of data

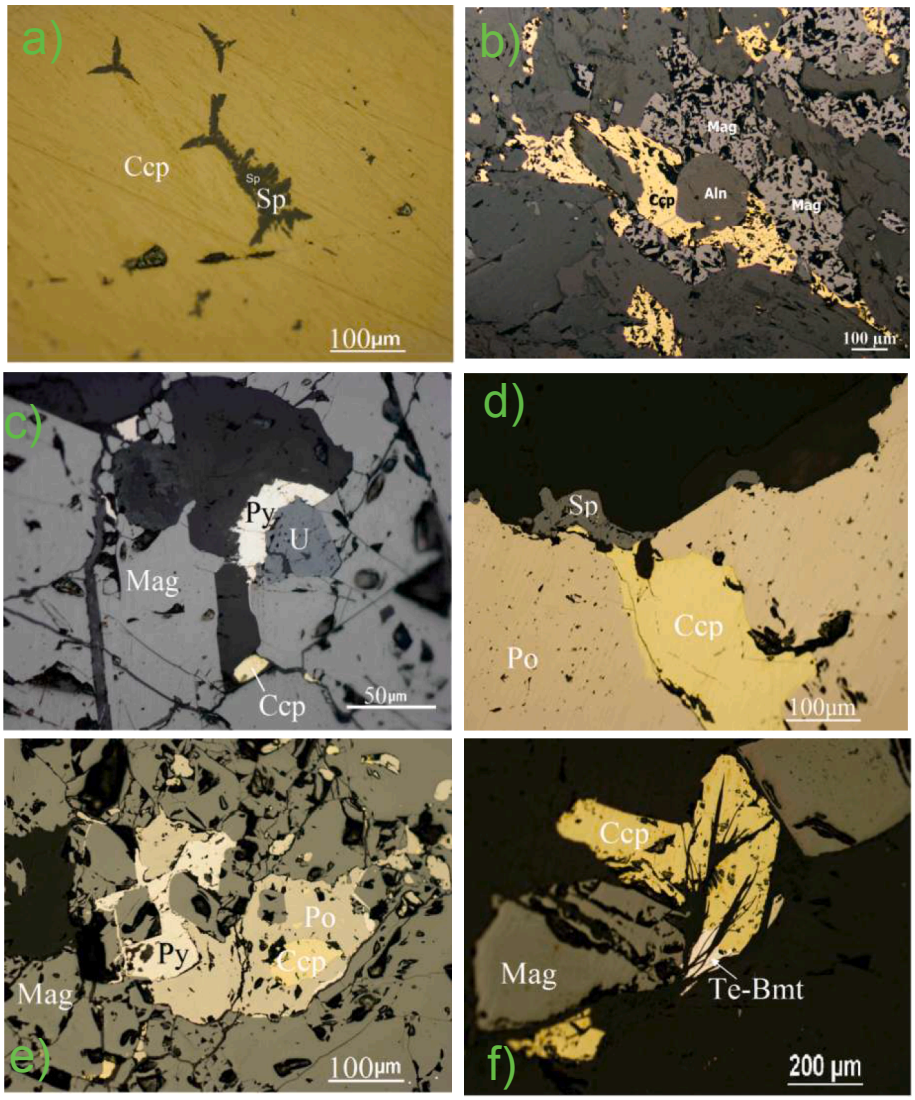


Fig. 9. a. Sphalerite (Sp) inclusion in chalcopyrite (Ccp), reflected light. b. Intergrowth of magnetite (Mag), chalcopyrite (Ccp); allanite(Al). Reflected light. c. Intergrowth of uraninite (U) with magnetite (Mag) and pyrite II (Py). Reflected light. d. Younger generation of sphalerite (Sp) in intergrowth with pyrrhotite (Po) and chalcopyrite (Ccp), reflected light. e. Pyrite (Py) pyrrhotite (Po) intergrowth with magnetite (Mgt), chalcopyrite (Ccp), reflected light. g. Te-Bismuthinite (Te-Bmt) with chalcopyrite (Ccp), reflected light.

acquisition from the sample. The off-line selection, integration of background and analysis of signals, time-drift correction and quantitative calibration for trace element analysis and U-Pb dating were performed using an Excel-based software ICP-MS Data Cal (Liu et al., 2008a, 2008b, 2010). Isoplot/Ex_ver3 was used to make the Concordia diagrams and weighted mean calculations (Ludwig, 2003). The result of U-Pb analysis of zircon for the intrusions and uraninite in ore minerals from the Sin Quyen mine is represented in Figs. 10, 12 and Table 1. U-Pb dating of uraninite from Sin Quyen deposits is represented in Fig. 11, and Table 2.

4.3. Ar/Ar dating

Samples were selected on the basis of their geological structure and freshness and investigated in thin polished sections. $^{39}Ar/^{40}Ar$ results were analyzed at Blaise Pascal University, France and the University of California. The results obtained were consistent in the two laboratories. K-feldspar, hornblende, biotite, and white mica mineral separations were obtained using fluid and magnetic separation techniques from heavily crushed fresh specimens. The purity of the final mineral separation was checked by binocular microscope. Feldspar, amphibole, and mica were irradiated with the Canyon sanidine (flux and salt monitors), in the Ford Reactor, University of Michigan. Various techniques have been applied to measure the age of mineral fractions: laser fusion or step by step heating. For samples treated by step-by-step heating, there is a common age spectrum from which the plateau and inverse isochron were calculated. If the isochron age is inversely close to the plateau age and $^{39}Ar/^{40}Ar$ is not significantly different from today's $^{39}Ar/^{40}Ar$ atmospheric ratio, the plateau age is reliable. When this is not the case, based on the inverse isochron, this is well defined. A particularly long schedule of fireplaces was underway on K-feldspar to obtain diffusion characteristics, apply diffusion models, and calculate thermal models. Comparable diffuse measurements on 115 K-feldspar confirmed that their activation energy defined a normal distribution with an average value of 46 ± 6 kcal/mol. In most cases, we also conduct two-stage isotherms heating step by step at low temperatures (450–800 °C); the first and second stages of the two long isothermal periods of order 10 and 15 min, respectively. Such heating schedules often produce a serrated age spectrum in which the second phase of the two periods is systematically younger and less affected by excess argon. The isochrons were also systematically inverted for K-feldspar. In some cases, careful interpretation of such cells, selecting linear arrays defined by a number of steps, can solve redundant argon problems in some parts of the age spectrum. When the age of a given mineral is calculated, a basic and controversial issue is to determine whether this age corresponds to the process of mineral crystallization, deformation or cooling under certain closing temperatures. This seems to be the case in most situations. The $^{39}Ar/^{40}Ar$ age corresponds to the age of cooling and the cooling history

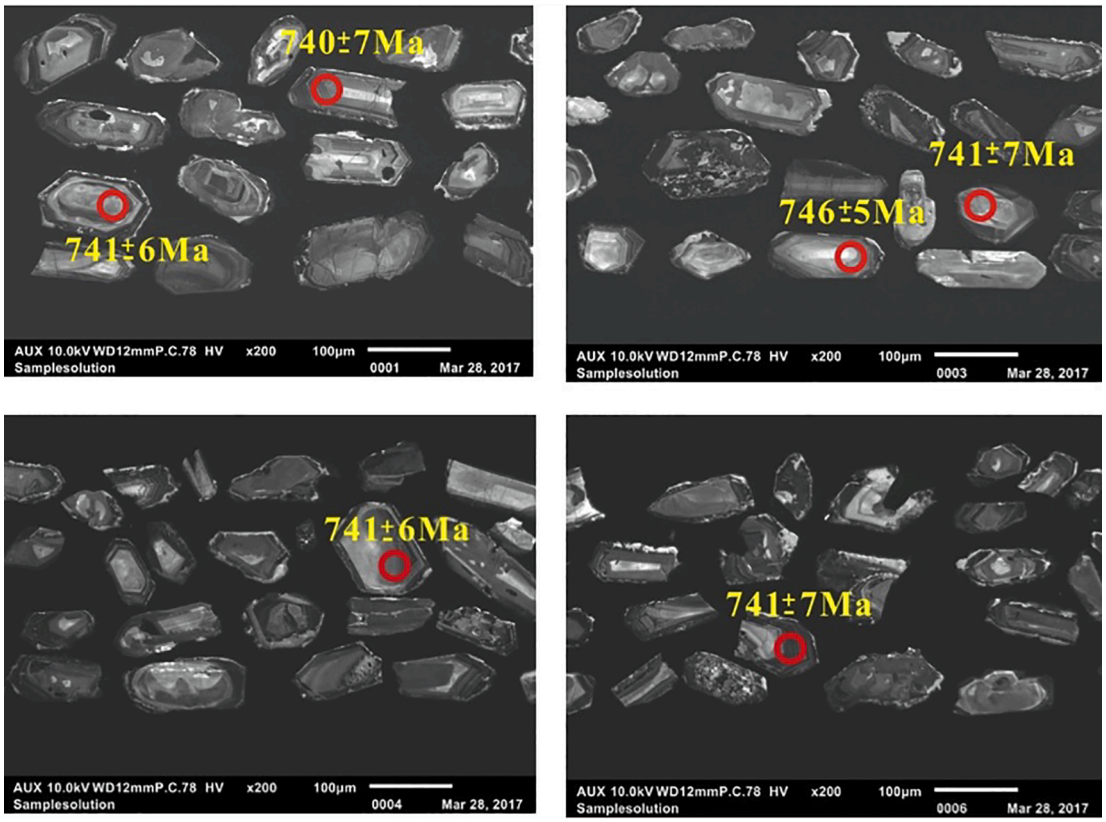


Fig. 10. Representative cathodoluminescent (CL) images of zircon grains, red circles show the location of LA-ICP-MS U-Pb analyses.

is systematically built up from the research results. This option leaves open discussion about the internal consistency of such cooling history and the relationship between 40 years old $^{39}Ar/^{40}Ar$ and deformed events. In fact, the $^{39}Ar/^{40}Ar$ of fine white mica may correspond to the synchronized kinematic crystalline age. It is assumed that there is a temperature of 320 ± 40 °C for biotite, 415 ± 40 °C for phlogopite, 390 ± 45 °C for white mica and 510 ± 50 °C for amphibole. As stated above, most of the feldspar K results come from calculation of cooling history using diffusion models. When such calculations were not possible, we quantitatively considered that the lower furnace temperature (400–700 °C) corresponds to cooling at 150–300 °C. Similarly, a well-defined plateau corresponds to employment cool slowly at these temperatures. The results of $^{39}Ar/^{40}Ar$ analysis of biotite and K-feldspar of the Baxat formation and Cu-Au Sin Quyen mine are represented in Fig. 13. We consider the age of this phase corresponds to the closing temperature of biotite of 320 ± 40 °C.

5. Discussions

5.1. Mineralization and timing

The underlying problem today is to determine whether the age corresponds to crystallization, deformation or cooling?

The $^{39}Ar/^{40}Ar$ ages, obtained from the Sin Quyen IOCG deposit, were consistent with ruby age along the Red River shear zone. The Ar-Ar age of ruby can be included in two different groups: the Miocene age group (from 23 to 24 Ma) from the DNCV samples in highly metamorphosed gneisses; 31 to 34 Ma ages in the Lo Gam area (Trinh et al., 1998; Garnier et al., 2002, 2008; Lien and Pho, 2018). The distribution of $^{39}Ar/^{40}Ar$ ages in various ruby mines in the Yen Bai and Luc Yen areas indicates older ages on the eastern part. There was no difference between syngenetic phlogopite related to ruby (31 to 32 Ma) and phlogopite and muscovite in marbles (31 to 34 Ma). These ages are different from the 23–24 Ma Ar - Ar ruby mineralization ages (Garnier et al., 2002).

In the DNCV range, deformations occurred under the amphibolite phase from 600 to 750 °C (Leloup et al., 2001). Moreover, the isotope thermometer in the Tan Huong mine shows a temperature of 600–625 °C (Giuliani et al., 1999, 2003). Since the crystallization of ruby is homologous with phlogopite formation, ruby forms above 600 °C, and graphite and calcite have coexisted with ruby and phlogopite. This temperature is higher than the temperatures calculated for phlogopite (385–455 °C), biotite (280–360 °C), and white mica (345–435 °C). Thus, the phlogopite age of 23–24 Ma represents the cooling age for the mica formed before this time, and therefore, the minimum age for ruby formation (Giuliani et al., 1999; Long et al., 2018; Huong et al., 2018). The temperatures for Ruby formation were between 630 and 745 °C. They are above the closing temperature of the mineral. Therefore, the Ar - Ar age for phlogopites also represents the age of cooling.

The Cenozoic intrusions belong to the Pu Sam Cap alkaline complex (33–35 Ma) and both the Jinshajiang-Red River and Jinping-Fanxipan alkaline porphyries (~40–30 Ma) (Tran et al., 2010a, 2014a; Liu et al., 2015; Leiluo et al., 2016; Findlay, 2018; Chau et al., 2016, 2017). The Cenozoic intrusions were formed almost together with ductile deformation in the ASRR Shear Zone at 38 ± 0.5 Ma based on $^{238}U/^{206}Pb$ (Garnier et al., 2005). Based on the results of the $^{39}Ar/^{40}Ar$ study by Leloup et al. (2001) and $^{238}U/^{206}Pb$ study by Liu et al. (2015), the Fanxinpan range was mostly dated at around 30 Ma. In the Lao Cai-Sapa section, the age ranged from about 88 to 21 Ma (Leloup et al., 2001). This stage was also noted by McLean (2001), Ishihara et al. (2011), Li et al. (2017), and the ages of ore mineralization and intrusions along the ASRR Shear Zone were confirmed and supported the recrystallization of the younger chalcopyrite and uraninite of Sin Quyen deposit at an age of no later than 21 Ma (Chung et al., 1997; Corrigan, 1991; Deng et al., 2015; Green et al., 1989; Harrison et al., 1996; He et al., 2015; Hu and Huang, 1997; Hu et al., 1995; Hurford, 1986; Leloup et al., 2001; Liang et al., 2002; Sun et al., 2007; Tianjian et al., 2019; Tran et al., 2010b,

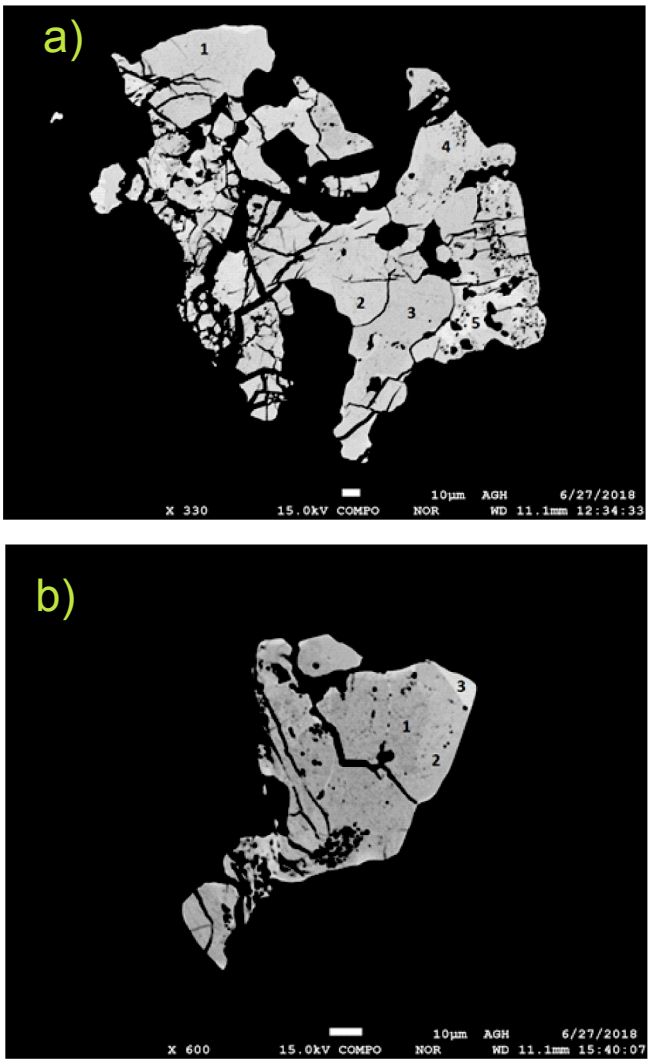


Fig. 11. The uraninite grains and points of absolute age determinations from the Sin Quyen mine.

2014b; Wang et al., 2001a, 2001b, 2005; Wang, 2005; Xu et al., 2012; Zhang et al., 2010, 2014a, 2014b; Zhen et al., 2017; Zhu et al., 2009, 2013).

The irregular K-feldspar $^{39}Ar/^{40}Ar$ age is interpreted by two episodes of rapid cooling: one at ~ 140 Ma and the other episodes from 41 to 25 Ma (Roger et al., 2000). The age of apatite fission tracks (33 Ma) indicated a rapid cooling event interpreted by the exhumation of the Chay river dome (Roger et al., 2000). The ages of the ASRR Shear Zone in this study and in previous studies are shown in Fig. 14 and Table 3. It can be seen that the result of the main timing of the mineralization in this study is almost consistent with that of previous studies.

In the Fanxipan zone, there were multi-staged plutonic intrusions (Tran et al., 2016): Neoproterozoic intrusions have been shown in the Ailao Shan – Fanxipan shear zone from 700 to 860 Ma (Liu et al., 2008a, 2008b, 2012a, 2012b, 2015; Wang et al., 2011; Qi et al., 2012; Wang et al., 2013; Cai et al., 2014, 2015; Li et al., 2015, 2017; Tran et al., 2016). But there is evidence that supports ages of 882 Ma for $^{206}Pb/^{238}U$ for the first REE mineralization with relevant magnetite and minor sulfite minerals of the Sin Quyen deposit from allanite and titanite associated with iron-oxide and Cu-Au ores (Dac et al., 2020). The period was also studied with a zircon and monazite age of 840–860 Ma, and high-temperatures of 460–590 °C (Li et al., 2017; Li and Zhou, 2018). They point out that the previous studies mentioned periods of multi-mineralization which were demonstrated with proofs of timing by high temperature minerals (zircon, monazite, allanite, and titanite) and indirectly relevant evidence from ore minerals (except Dac et al., 2020 but only mentioned for the earlier period) (Gaskov et al., 2012; Li et al., 2017; Li and Zhou, 2018; Liu and Chen, 2019).

Collisions between the Indochina and China blocks strongly affected the tectonic structure in a large area of northern - Vietnam (Jian et al., 2009). The tectonic units of the Red River zone, Day Nui Con Voi ridge, Chay River zone, Fanxipan uplift, Tu Le belt, Da River zone, and Ma River zone were mentioned with a timing range from 270 to 230 Ma (Gilley et al., 2003; Pham et al., 2008, 2013; Balykin et al., 2010; Tong-Dzuy and Vu, 2011; Zhang et al., 2013; Hieu et al., 2013; Faure et al., 2014; Usuki et al., 2015). The 249 to 259 Ma determined from late Permian to Early Triassic intrusions include the Muong Hum, Phu Sa Phin, Fanxipan-Posen, Ye Yen Sun, Nam Xe –Tam Duong granitoids (Pham et al., 2013, 2020; Usuki et al., 2015). As regards intrusion activities, numerous Fe-Cu, and IOCG deposits were formed at different stages in relation to multiple hydrothermal events. The majority of the deposits are located in southwestern China along the ASRR shear zone, i.e., Yinachang Fe-Cu-REE deposit. There were four stages of mineralization: sodic alteration; magnetite mineralization; Cu sulfide with REE mineralization and final barren calcite veining. In the north-west of the Sin Quyen district, there is the Suoi Thau Cu deposit (Fig. 2). Herein, there were three stages of alteration and mineralization: potassic alteration; silicification mineralization; and phyllic alteration (Tran et al., 2016).

Based on age determination by the U-Pb method and previous publications on the IOCG Sin Quyen deposit, it is suggested that there are two distinct phases of mineralization:

a. Metasomatic alteration phase: We accept the results of previous studies, although we found that the distribution shows a great dispersion over time of periods when mineralization took place. We also suspect that the age of zircon or uraninite corresponds to the age of the iron-gold deposits due to the closed temperature of zircon and uraninite is high. The spatial distribution of allanite, magnetite, and ore minerals is closely related to the metasomatic fluids derived from oxidized magma (McLean, 2001; Ta et al., 1975; Ishihara et al., 2011).

The first stage is the time when Na-K alteration takes place in amphibolite and granite-gneiss (Ta et al., 1975). In the second stage, allanite is depleted of mafic components with epidote intergrowths in crystals and linked to the epidote by the coupled substitution of $REE^{3+}+Fe^{2+} \Leftrightarrow Ca^{2+}+Fe^{3+}$ (Ishihara et al., 2011)

The third stage is the alteration from mafic liquids derived from an oxidized source magma to younger altered formations (Ta et al., 1975; Ishihara et al., 2011). This stage formed the major ore minerals of magnetite-allanite-uraninite (Pieczonka et al., 2019). This stage lasted from 744 ± 3 Ma to 520 ± 40 Ma, documented by the age of zircon (Table 1, Fig. 12) and uraninite measured using U-Pb methods (Table 2, Fig. 11, Pieczonka et al., 2019). Based on previous studies one can state that the period would have had a high temperature from 450 to 610 °C for precipitation of uraninite to zircon (Gaskov et al., 2012; Li et al., 2017; Li and Zhou, 2018; Yuan et al., 2019).

Wavelength-Dispersive X-Ray Spectroscopy was used for analyses and mineral age calculations (Table. 2). The composition of uraninites depends on the amounts of REE. The presence of REE in the uraninites suggests a simultaneous process of crystallization of both REE and uranium. There are two types of uraninites depending on their U-Pb dating: old uraninites dated as 520 Ma old with elevated REE content (up to 8 wt %) and with high lead content (up to 6.8 wt%) and younger uraninites <88 Ma with much lower contents of REE (less than 2.7 w.%) and Pb

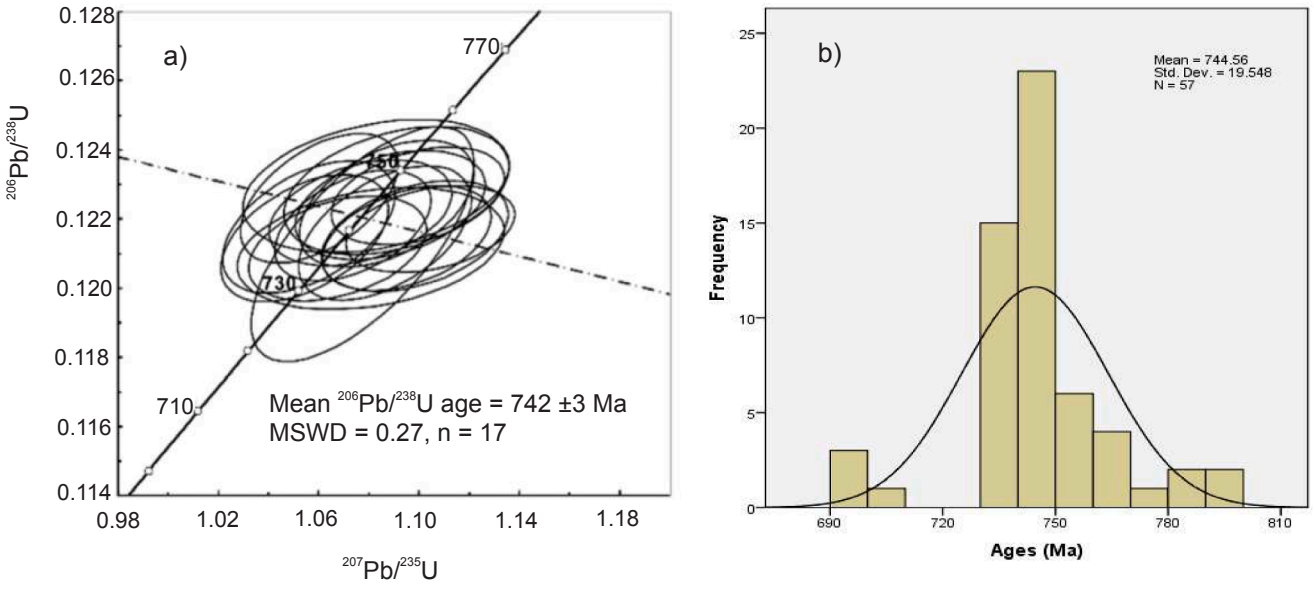


Fig. 12. a. Zircon U-Pb concordia diagrams for the intrusions from the Sin Quyen mine. b. Histogram of the distribution of the age of zircon around 744 Ma in the Sin Quyen deposit.

Table 1
In situ LA-ICP-MS U-Pb data for zircon from intrusions in the Sin Quyen mine.

No	Th	U	$^{207}Pb/^{206}Pb$	$^{207}Pb/^{206}Pb$	$^{207}Pb/^{235}U$	$^{207}Pb/^{235}U$	$^{206}Pb/^{238}U$	$^{206}Pb/^{238}U$
			Ratio	1sigma	Ratio	1sigma	Ratio	1sigma
SQ1	165	803	0.0637	0.0012	1.0738	0.0205	0.1218	0.0011
SQ2	242	531	0.0647	0.0014	1.0865	0.0228	0.1216	0.0013
SQ3	152	345	0.0647	0.0013	1.0996	0.0228	0.1227	0.0009
SQ4	235	506	0.0626	0.0012	1.0562	0.0227	0.1218	0.0013
SQ5	194	377	0.0652	0.0013	1.0952	0.0222	0.1214	0.0010
SQ6	236	531	0.0629	0.0013	1.0546	0.0220	0.1214	0.0012
SQ7	163	346	0.0643	0.0013	1.0874	0.0229	0.1224	0.0012
SQ8	42	120	0.0638	0.0020	1.0830	0.0351	0.1230	0.0013
SQ9	276	294	0.0641	0.0016	1.0913	0.0296	0.1228	0.0012
SQ10	155	333	0.0637	0.0014	1.0677	0.0235	0.1212	0.0010
SQ11	134	305	0.0646	0.0015	1.0886	0.0251	0.1224	0.0010
SQ12	127	387	0.0637	0.0014	1.0768	0.0241	0.1222	0.0010
SQ13	39	102	0.0650	0.0022	1.0810	0.0351	0.1211	0.0012
SQ14	221	368	0.0656	0.0013	1.1046	0.0223	0.1217	0.0008
SQ15	79	407	0.0644	0.0016	1.0775	0.0293	0.1213	0.0022
SQ16	195	503	0.0653	0.0014	1.0986	0.0245	0.1215	0.0011
SQ17	174	529	0.0626	0.0012	1.0605	0.0208	0.1226	0.0012

$^{207}Pb/^{206}Pb$	$^{207}Pb/^{206}Pb$	$^{207}Pb/^{235}U$	$^{207}Pb/^{235}U$	$^{206}Pb/^{238}U$	$^{206}Pb/^{238}U$	Concordance
Age (Ma)	1sigma	Age (Ma)	1sigma	Age (Ma)	1sigma	
731	36	741	10	741	6	99%
765	46	747	11	740	7	99%
765	43	753	11	746	5	99%
694	43	732	11	741	7	98%
783	47	751	11	739	6	98%
706	43	731	11	739	7	98%
750	42	747	11	745	7	99%
744	67	745	17	748	7	99%
746	49	749	14	747	7	99%
731	45	738	12	737	6	99%
761	44	748	12	744	6	99%
731	52	742	12	743	6	99%
776	77	744	17	737	7	99%
792	43	756	11	740	5	97%
767	54	742	14	738	13	99%
783	42	753	12	739	6	98%
694	43	734	10	746	7	98%
694	36	731	10	737	5	**Min**
792	77	756	17	748	13	**Max**
748	**48**	**744**	**12**	**742**	**7**	**Aveg**

Table 2
An example of some uraninite WDS measurements and age calculation.

points	ThO2	UO2	PbO	Age [Ma]	position on Fig. 9 a, b
0005	0.034	85.047	6.388	**538**	AP464_fot3a_p1
0006	0.075	84.474	6.849	**578**	AP464_fot3a_p2
0007	0.000	98.728	0.755	**57**	AP464_fot3a_p3
0008	0.000	82.875	7.191	**616**	AP464_fot4_p1
0009	0.000	84.084	6.414	**545**	AP464_fot4_p2
0010	0.103	82.761	6.752	**581**	AP464_fot4_p3
0011	0.000	83.510	6.127	**526**	AP464_fot4_p4
0012	0.166	94.027	0.680	**54**	AP464_fot4_p5

(less than 1.1 w.%) (Table. 2) (Pieczonka et al., 2019). Those two types of uraninite are also clearly visible in the Back Scattering Electron image (Pieczonka et al., 2019). There are probably two sources of uraninites in the Sin Quyen deposit: hydrothermal and metamorphic. U-Pb dating of uraninites can support the dating of both the hydrothermal and metamorphic sources (Ta et al., 1975). The CL images are shown in Fig. 10 in which the zircon cores mostly present sector or oscillatory zoning. Clear sectors or oscillatory zoning are seen at seventeen spots. The results show moderate to high concentrations of Th (39 to 276 ppm) and U (102 to 803 ppm), with ratios of Th/U varying from 0.2 to 0.9 (Table 1). The seventeen concordant analyses cluster together and yield a weighted average $^{206}Pb/^{238}U$ age of 744 ± 3 Ma (MSWD = 0.27) (Fig. 12), which is interpreted as the emplacement age of the Sin Quyen intrusion.

Before the hydrothermal phase from the late Permian to the Middle Triassic, there were collisions between the Indochina and China blocks which were mentioned above. However, the effects of the collision between the Indochina and South China blocks and later cooling time on the SQF were not observed (Mclean, 2001; Ishihara et al., 2011).

On the other side of the Red River Shear Zone (Song Chay zone), U/Pb dating yields a 428 Ma age for the granite crystallization (Roger et al., 2000). Rb/Sr on white micas and biotite yielded ages from 206 to 176 Ma, whereas the $^{39}Ar/^{40}Ar$ rages of the same minerals are from 210 to 190 Ma (Roger et al., 2000). Various formation ages on both sides of the Red River fault zone show that the Sin Quyen deposit, located in a zone with a long history of tectonic development and with a last mineralizing episode, was related to Cenozoic left-lateral motion along the Red River shear zone. The formation mechanism in the first phase of the Sin Quyen deposit is unclear due to high-temperature deformation in the Cenozoic that can remove the evidence for low-temperature mineralization. We recognize many peaks of ages in the synthetic histogram of the age of the Sin Quyen deposit (Fig. 15) (Li et al., 2017; Pieczonka et al., 2019; Dac et al., 2020). It is possible that identifying the age of zircon, uraninite, and titanite gave us the dating of tectonic, metamorphic or magmatic events.

b. Hydrothermal phase:

The age of K-feldspar and uraninite at 70–88 Ma corresponds to the first stage of cooling. These results are consistent with the age of the IOCG deposits along the Red River Shear Zone (Figs. 15, 16). Biotite data clearly indicate the age and temperature of ore formation. Although the spectrum of K-feldspar is not as clear as the biotite spectrum, it anyway yields some age evolution. We can distinguish 3 stages of 25–26 Ma, 35 Ma and 88 Ma in the K-feldspar spectrum. We obtained 25 Ma and 34 Ma from the K- feldspar inverse isochron. The age of 34–35 Ma determined from K- feldspar is in accordance with the age of biotite. The spectrum of K- feldspar is quite complex, which can be explained by the uplift of the Red River shear zone. The age of 70–88 Ma for K- feldspar and uraninite determined by U-Pb dating corresponds to the first stage of cooling. That is why we consider the formation of the IOCG Sin Quyen deposit corresponds to a biotite age of 33–35 Ma at the temperature of 320 ± 40 °C.

Sulfides are formed and gold is deposited during a later hydrothermal stage, mainly in schist, granite-gneiss, and amphibolite (McLean, 2001; Ta et al., 1975). This phase forms a mineral, that is rich in chalcophile elements with positive correlation coefficients (Hao, 2018). The sulfur of both sulfides from the first and second phase originated from a deep-level source with a stable isotopic composition $\delta^{34}S$ from −2.5 to + 1.3‰ following Gaskov et al. (2012) and from −2.78 to + 8.65‰ (Pieczonka et al., 2019).

The phase begins with quartz-molybdenite penetrating altered rocks (Ta et al., 1975). Those minerals are particularly observed in the northwestern part of the deposit, where plagiogranites are present.

The phase formed chalcopyrite-pyrrhotite-pyrite mineral groups from oxygen-rich hydrothermal liquid in the 300–500 °C temperature range (Ta et al., 1975; Krismer et al., 2011; Sugaki et al., 1989, 1987; Leloup et al., 2001; Garnier et al., 2002, 2005; Hao, 2018) with a sphalerite inclusion in chalcopyrite (Fig. 9a). In addition, as reported by Ishihara et al. (2011), the ores are often gathered together in felsic zones comprised of detrital and recrystallized quartz and feldspars, and dark greenish zone including pyroxene, amphibole, biotite and allanite-epidote. This period started from the recrystallization of younger 22 and 88 Ma chalcopyrite and uraninite (Figs. 11, 13 and Pieczonka et al., 2019), which came from rich volatile hydrothermal fluids at high temperature (300 °C−500 °C). The temperature was estimated to be lower than the ruby mineralization phase, with inter-grown chalcopyrite and quartzite vein filling in fractures in magnetite minerals, and ore minerals filling in fractures in quartz and calcite, and actinolite-altered skarn hornblende (Fig. 8a-d). $^{39}Ar/^{40}Ar$ study of biotite and K-feldspar in the Baxat formation and Sin Quyen deposit yielded 33–35 Ma for biotite and 25–35 Ma to 22–88 Ma for K-feldspar (Fig. 13). We consider that the formation of the Sin Quyen IOCG deposit corresponds to a biotite age of 33–35 Ma at the temperature at 320 ± 40 °C. This age was cited for the latest 30 Ma Cu-Au mineralization ($^{87}Sr/^{86}Sr$) (Li et al., 2017). The age of K-feldspar and uraninite at 70–88 Ma corresponds to the first stage of cooling. A cooling temperature was suggested within the range from 250 to 450 °C for re-precipitation of uraninite (Yuan et al., 2019). These results are consistent with the age of the IOCG deposits along the Red River Shear Zone (Figs. 15, 16).

5.2. *Kinematic model of the formation of the Sin Quyen and other IOCG deposits*

Based on the pressure–temperature conditions and ages of the deposits, the distribution of Sin Quyen and other IOCG deposits along the Red River and their ore structure coincides with the foliation planes, a model is proposed for the formation of the Sin Quyen and IOCG deposits in the Cenozoic. In this model, the clockwise rotation of the Indochina block produced three different zones. The first zone is in a compressive regime, the second zone is in a pure strike-slip regime, and the third one was in an extensional regime (Fig. 17). In this model called the "Zipper model", the Sin Quyen and the other IOCG deposits occurred within the pure strike-slip zone, extending for several hundred kilometers along the Red River shear zone.

This model is also applied to ruby formation. Ruby deposits formed at the frontier of the pure strike-slip zone and the extensional zone, but at deeper levels at temperatures of 700–800 °C.

The Zipper model was first proposed by Trinh et al. (1994) and then developed by Harrison et al. (1996) and Leloup et al. (2001). The Red River shear zone experienced a left lateral movement. Assuming the South China block is fixed, then the Indochina block rotated clockwise. If the Red River shear zone is a transform fault, it would follow a small circle of the Euler rotation pole between the Indochina and South China blocks, and the movement would be purely strike-slip, if the fault does not follow a small circle. A compressive regime will be found in the

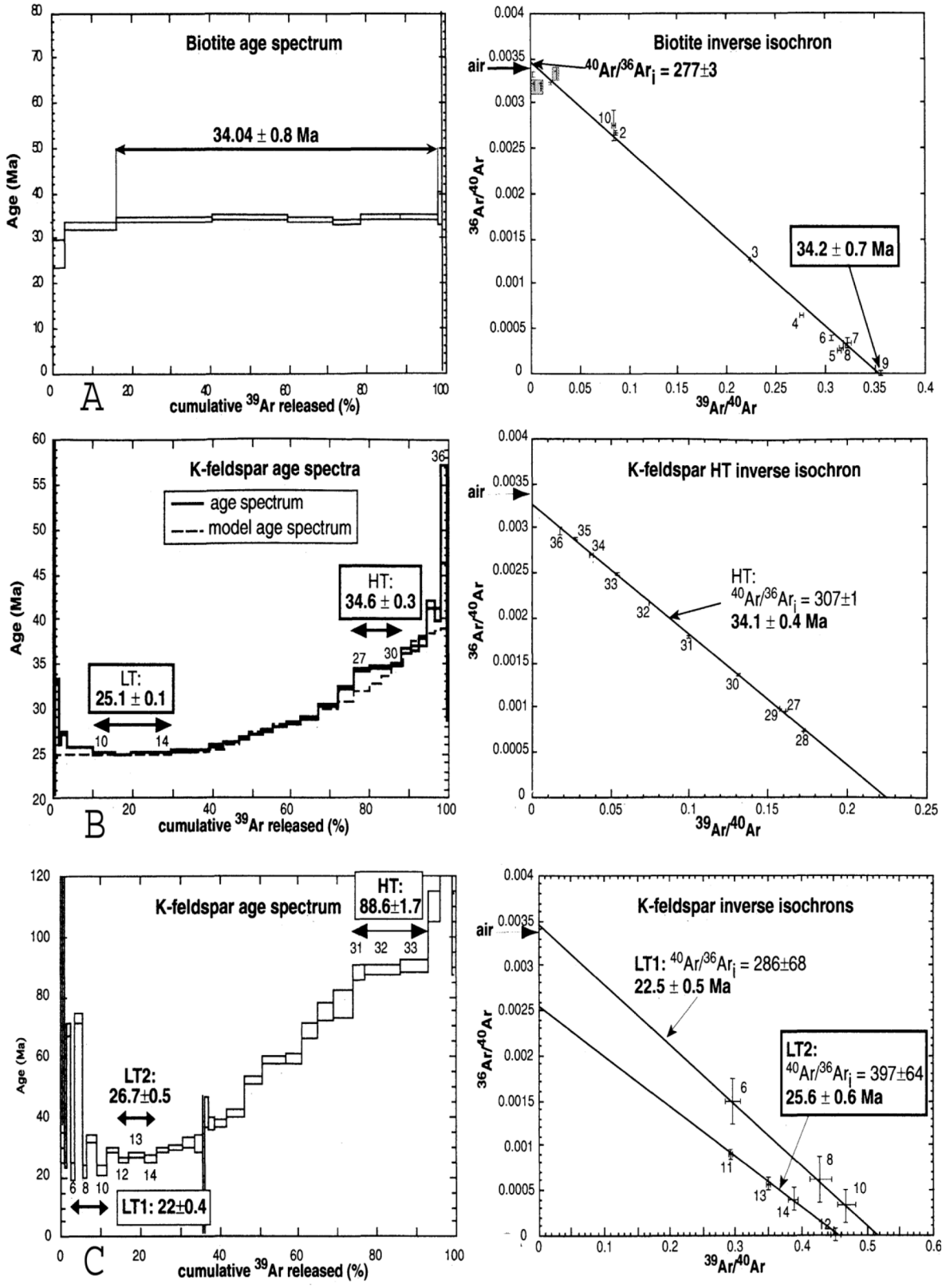


Fig. 13. The timing of the Baxat formation and the Sin Quyen Cu-Au Mine. a. $^{39}Ar/^{40}Ar$ dating of biotite mineral. b, c. $^{39}Ar/^{40}Ar$ dating of K-feldspar age spectrum and inverse isochrons (modified from Leloup et al., 2001).

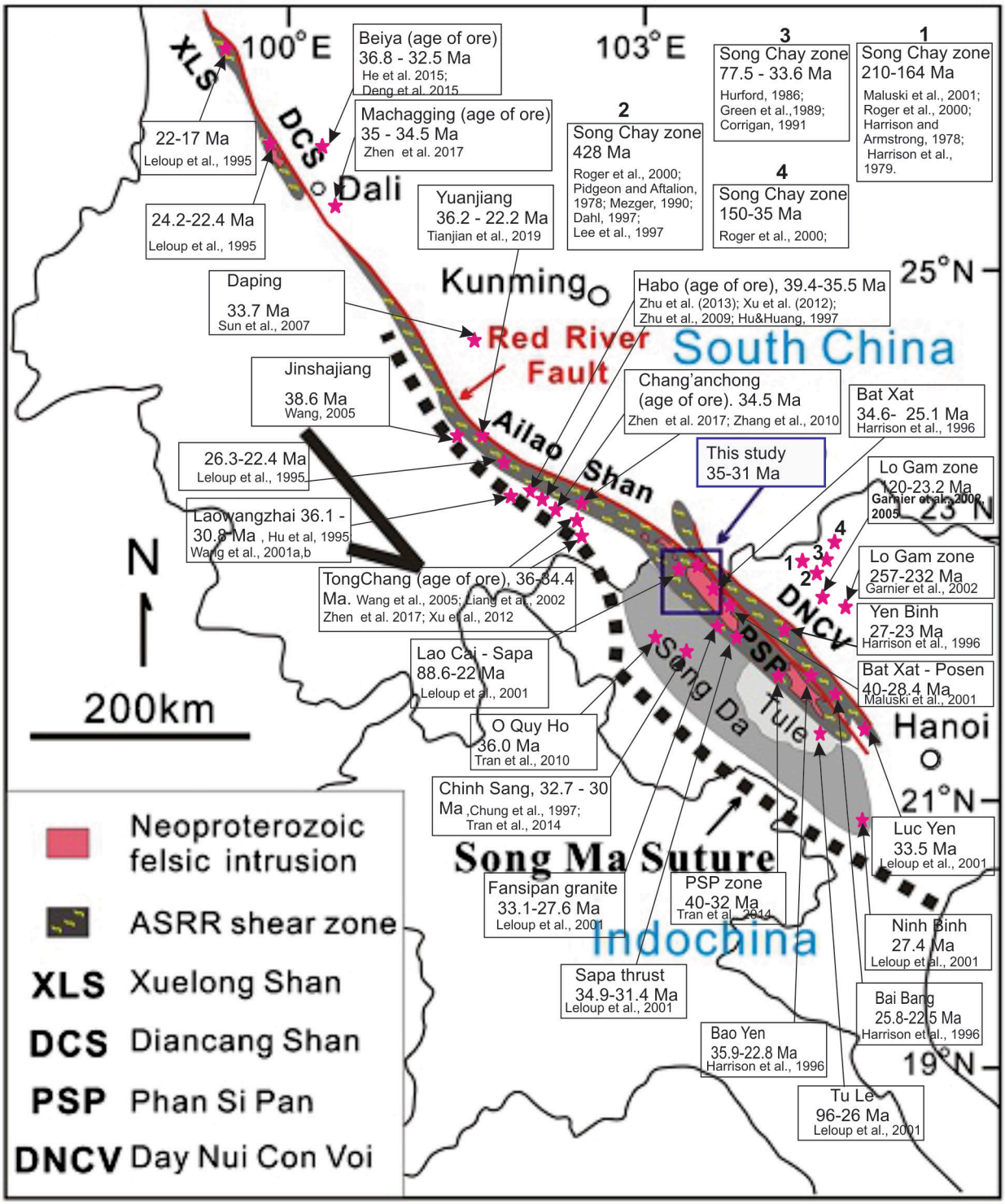


Fig. 14. The distribution of massive intrusions and IOCG deposits along the Ailao Shan - Red River shear zone.

Tab. 3
Summary of geochronology of representative porphyry deposits and introsion rocks along Ailao Shan-Red River shear zone.

Deposit/Site	Location	Intrusion type	Minerals	Method	Age of ore/ intrusive rock	References
Beiya	Heqin region, Yunnan, China	Quartz, monzonite, porphyry	Molybdenite, phlogopite	Re–Os $^{39}Ar/^{40}Ar$	36.8–32.5 Ma	He et al. (2015), Deng et al. (2015);
Tongchang	Jinping region, Yunnan, China	Quartz syenite, porphyry	Molybdenite	Re–Os Re–Os	34.4 Ma	Xu et al. (2012); Zhen et al. (2017)
Chang'anchong	Jinping region, Yunnan, China	Quartz, monzonite, granite	Molybdenite, Zircon	Re–Os U-Pb	34.5 Ma	Zhen et al. (2017)
Habo	Yuanyang region, Yunnan, China	Quartz, monzonite, porphyry	Molybdenite, Zircon	Re–Os U-Pb	35.5 Ma	Zhen et al. (2017); Zhu et al.0 (2013); Xu et al. (2012)
Chang'an	Jinping region, Yunnan, China	Syenogranite porphyry	Molybdenite, Zircon	Re–Os U-Pb	33.3 Ma	Zhen et al. (2017), Zhang et al. (2014a), Zhang et al. (2014b)
Yuanjiang	Jianshui region, Yuanjiang, China	calcite-rich marble (phlogopite, scapolite, graphite, pyrite)	Phlogopite, Zircon	$^{39}Ar/^{40}Ar$ U-Pb	36.2–22.2 Ma	Tianjian et al. (2019)
Bat Xat	$22^0$32′ 56″ N $103^0$47′ 20″ E	Orthogneiss, quartz mylonite	Biotite, Kf	$^{39}Ar/^{40}Ar$	34.6–28.1 Ma	Harrison et al. (1996)
Lao Cai - Sapa	$22^0$21′ 53″ N $103^0$56′ 33″ E	Orthogneiss, quartz mylonite	Biotite, Kf	$^{39}Ar/^{40}Ar$	88.6–22 Ma	Harrison et al. (1996), Leloup et al. (2001)
Sapa thrust	$22^0$20′ 18″ N $103^0$51′ 15″ E	Marble, amphibolite	Biotite Phlogopite	$^{39}Ar/^{40}Ar$	35.3–32.4 Ma	Leloup et al. (2001)
PSP granite	$22^0$21′ 43″ N $103^0$45′ 40″ E	Fine-granined granite, leucocratic dike	Kf	$^{39}Ar/^{40}Ar$	33.5–27.4 Ma	Leloup et al. (2001)
Tu le	$22^0$02′ 07″ N $104^0$00′ 19″ E	Rhyolite	Kf	$^{39}Ar/^{40}Ar$	33.3 Ma	Leloup et al. (2001)
Bao Yen	$22^0$13′ 27″ N $104^0$27′ 17″ E	Orthogneiss, mylonite paragneiss	Biotite, Kf	$^{39}Ar/^{40}Ar$	35.9–22.8 Ma	Harrison et al. (1996) , Leloup et al. (2001)
Luc Yen	–	Marble	Phlogopite	$^{39}Ar/^{40}Ar$	33.5 Ma	Leloup et al. (2001)
Yen Binh	$21^0$47′ 10″ N $104^0$54′ 15″ E	Mylonitic garnet micaschist with leucocratic veins	Biotite, Kf	$^{39}Ar/^{40}Ar$	27.3–21.7 Ma	Harrison et al. (1996), Leloup et al. (2001)
Bai Bang	$21^0$24′ 20″ N $105^0$18′ 39″ E	Mylonitic garnet, micaschist	Biotite, Kf	$^{39}Ar/^{40}Ar$	25.8–22.5 Ma	Harrison et al. (1996), Leloup et al. (2001)
Ninh Binh	$20^0$19′ 47″ N $106^0$04′ 34″ E	Mylonitic garnet, micaschist	Biotite	$^{39}Ar/^{40}Ar$	27.4 Ma	Leloup et al. (2001)
Lo Gam zone	An Phu, Lo Gam area	Granite	Zircon, Biotite	$^{39}Ar/^{40}Ar$ U-Pb	120–23.2 Ma	Garnier et al. (2002), Garnier et al. (2005)
Lo Gam zone	Minh Tien, Lo Gam area	Granite	Zircon	U-Pb	257–232 Ma	Garnier et al. (2002)
Song Chay zone	Song Chay area	Granite	Zircon, Biotite, Muscovite	U-Pb, Rb/Sr, $^{39}Ar/^{40}Ar$	210–164 Ma	Maluski (2001), Roger et al. (2000), Purdy and Jager (1976), Cliff (1985), Dodson (1973), Hames and Bowring (1994), Harrison (1978, 1979)
Song Chay zone	Song Chay area	Granite	Zircon	U-Pb	428 Ma	Roger et al. (20000, Pidgeon and Aftalion (1978), Mezger (1990), Lee et al. (1997)
Song Chay zone	Song Chay area	Granite	Zircon, Apatite	U-Pb	77.5–33.6 Ma	Hurford (1986), Green et al. (1989), Corrigan (1991)
Song Chay zone	Song Chay area	Granite	K-feldspar	$^{39}Ar/^{40}Ar$	150 – 35 Ma	Roger et al. (2000)
Laowangzhai	–	Lamprophyre	Phlogopite	$^{39}Ar/^{40}Ar$	36.1–30.8 Ma	Hu et al. (1995), Wang et al. (2001a), Wang et al. (2001b)
Jinshajiang	–	Ore	Quartz	$^{39}Ar/^{40}Ar$	38.6 Ma	Wang (2005)
Habo area	–	Syenite porphyry, Quartz porphyry, Ore, Syenite porphyry, Quartz syenite	Zircon, Molybdenite, Whole rock	U–Pb, Re–Os, Rb–Sr	39.4–35.5 Ma	Zhu et al. (2009), Hu and Huang (1997)
Tongchang	–	Syenite porphyry, Quartz syenite porphyry, Ore	Zircon, Molybdenite	U–Pb, Re–Os	34.3–36 Ma	Wang et al. (2005), Liang et al. (2002)
Daping	–	Sericite-quartzite	Sericite	$^{39}Ar/^{40}Ar$	33.7 Ma	Sun et al. (2007)
Chang'an	–	Lamprophyre	Biotite	$^{39}Ar/^{40}Ar$	35.2 Ma	Zhang et al. (2010)
O Quy Ho	–	Ore	Molybdenite	Re–Os	36.0 Ma	Tran et al. (2010a), Tran et al. (2010b)
Chinh Sang	–	Trachyte, Syenite	Phlogopite, Zircon	$^{39}Ar/^{40}Ar$, U–Pb	32.7–30 Ma	Chung et al. (1997), Tran et al. (2014a), Tran et al. (2014b)
Sin Quyen	Sinh Quyen, Bat Xat, Lao Cai	Amphibolite, Quartz, Skarn, porphyry Biotite, K-Fendspar	Zircon, Titanite Uraninite Biotite, K-Fendspar	U-Pb $^{39}Ar/^{40}Ar$	742–500 Ma 70 Ma 34 Ma 84–22 Ma	This study

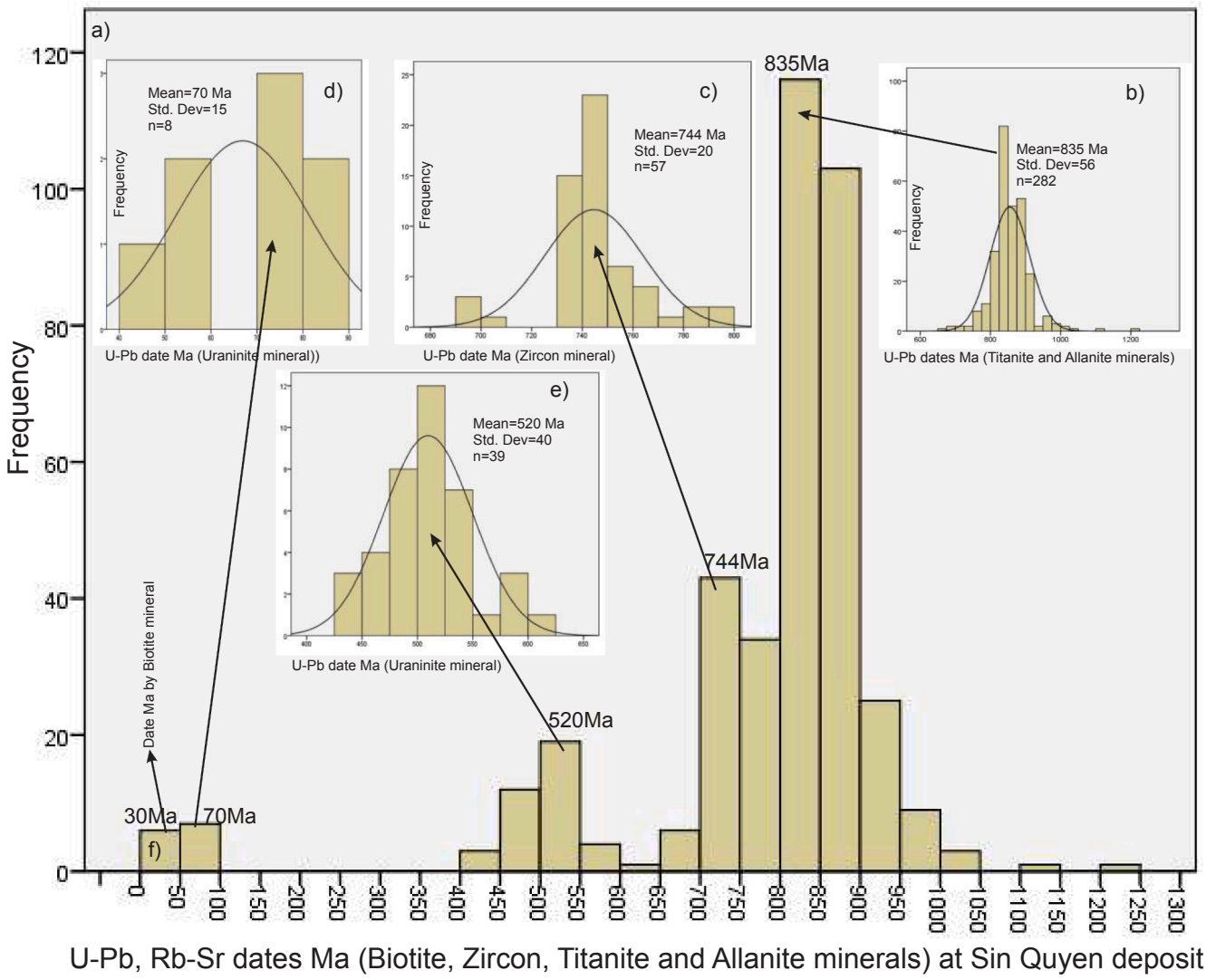


Fig. 15. a. Synthetic histogram of mineral ages in the Sin Quyen deposit; b. Synthetic histogram of minerals of zircon, titanite, allanite U-Pb age (Li et al., 2017; Dac et al., 2020); c: Histogram of U-Pb age for uraninite (This study); d, e: Synthetic histogram of U-Pb age of uraninite (This study and Pieczonka et al., 2019); f: Timingby Biotite mineral (Li et al., 2017).

northwest border and an extensive regime will be found in the southeast border of the Red River Shear Zone.

6. Conclusions

The Sin Quyen IOCG deposit is controlled by the Sin Quyen reverse fault, as well as Pin Ngan Chai, and Thung Sang faults. All of these are parallel and are demonstrated to be splays of the Red River fault zone. Copper ore is mainly hosted within contact with amphibolites and the granite-gneiss zone in sedimentary and metamorphic rocks of the Sin Quyen formation.

The mineralization corresponding to the fracture phases can be divided into two principal phases: i) a 744–520 Ma metasomatic alteration phase forming magnetite, uraninite, and allanite in many intrusion; ii) hydrothermal sulfide phases. This event formed chalcopyrite, pyrrhotite, and pyrite mineral groups in the temperature range 320 ± 40 °C between 22 and 88 Ma, most likely at 31–35 Ma along the ASRR Shear Zone. This phase was started by heating due to Cenozoic left-lateral motion along the Red River shear zone which made sulfur minerals crystallize far enough from the center of tectonic activity. At the end of this phase, many iron, copper, and gold deposits were formed along the ASRS zone. The zipper tectonic model can explain the formation of Sin Quyen and other IOCG along the Red River Shear Zone, formed within the pure strike-slip fault zone.

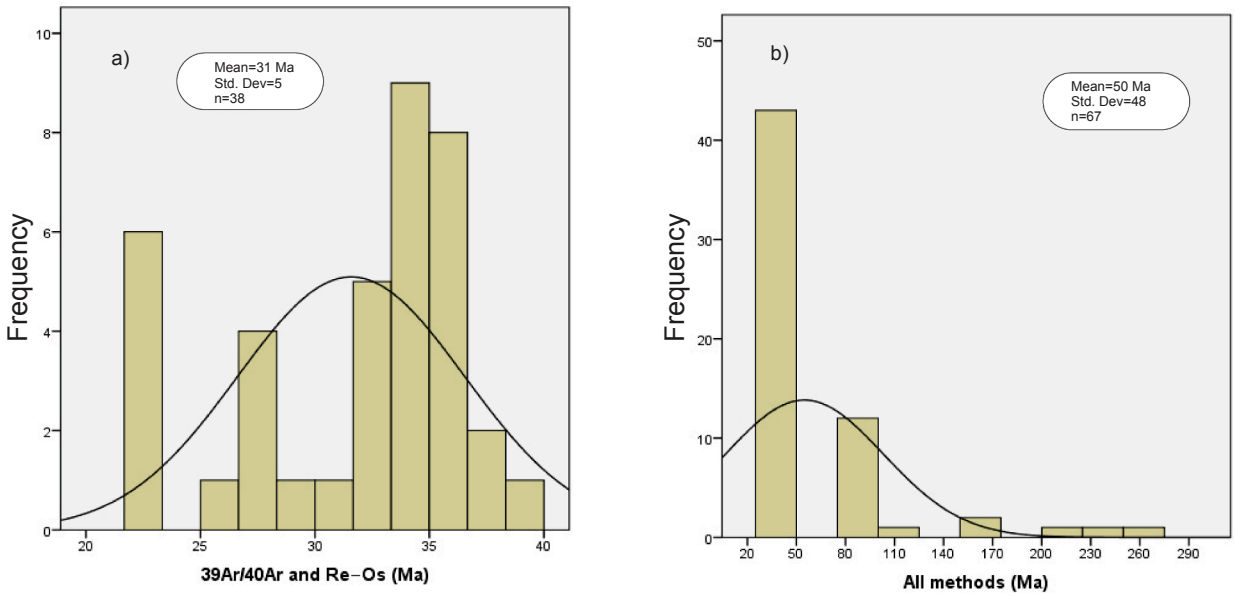


Fig. 16. Timing historical histogram of IOCG deposits along the Ailao Shan - Red River shear zone.

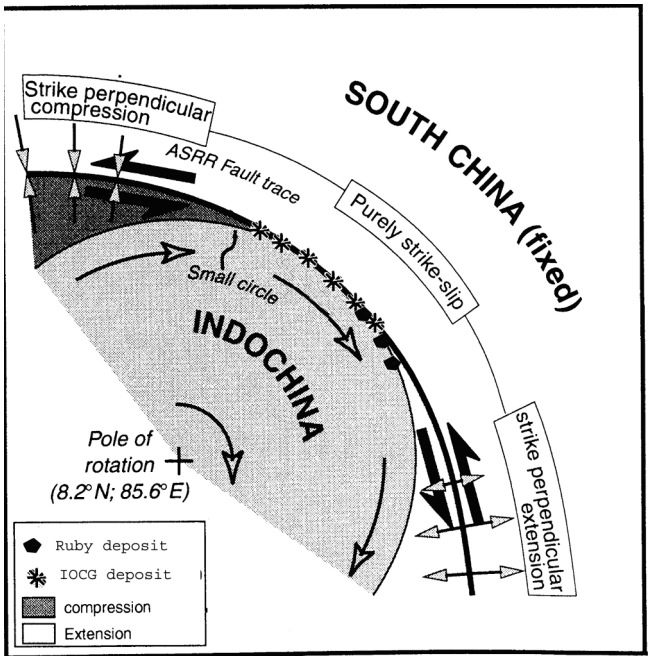


Fig. 17. The zipper tectonic model for ruby and IOCG mineralization along the Red River shear zone within the ASRR fault line. IOCG deposits occurred along the purely strike-slip Cenozoic shear zone in lower pressure–temperature environment while ruby deposits occurred along the Cenozoic extensional strike-slip shear zone in higher pressure–temperature (modified from Trinh et al., 1994, Leloup et al., 2001).

Declaration of Competing Interest

The authors declare that they have no known competing financial interests or personal relationships that could have appeared to influence the work reported in this paper.

Acknowledgments

Nguyen Dinh Chau thanks the bilateral cooperation between Hanoi University of Mining and Geology (HUMG) and AGH University of Science and Technology. Phan Trong Trinh thanks the national project "Study of Pliocene to present-day tectonics in the Vietnam Continental shelf for assessment of geological hazards", KC.09.22/16-20. The second author would like to thank Professors Tapponnier and Leloup for providing the data from the cooperation project between the Vietnam Academy of Science and Technology (VAST) and CNRS, France, and the research support for the senior Researcher (VAST), Code: NVCC 11.01/21.

Appendix A. Supplementary data

Supplementary data to this article can be found online at https://doi.org/10.1016/j.oregeorev.2021.104065.

References

Anczkiewicz, R., Viola, G., Müntener, O., Thirwall, M.F., Villa, I.M., Cuong, N.Q., 2000. Evolution of the Red River Shear Zone deduce from structural and Fission track studies of the Day Nui Con Voi massif in North Vietnam. Mineral. Soc. Poland Spec. Pap. 17, 108–110.

Anczkiewicz, R., Viola, G., Muntener, O., Thirlwall, M.F., Villa, I.M., Quong, N.Q., 2007. Structure and shearing conditions in the Day Nui Con Voi massif: implications for the evolution of the Red River shear zone in northern Vietnam. Tectonics 26, TC2002. https://doi.org/10.1029/2006TC001972.

Balykin, P.A., Polyakov, G.V., Izokh, A.E., Tran, T.H., Ngo, T.P., Tran, Q.H., Petrova, T. E., 2010. Geochemistry and petrogenesis of Permian ultramafic-mafic complexes of the Jinping-Song Da rift (southeastern Asia). Russ. Geol. Geophys. 51, 611–624.

Bui, P.M., Nguyen, V.H., Phan, V.K., Tran, D.T., 2004. Geology and mineral resources of Kim Binh-Lao Cai sheet. Scale 1:200,000, Dept. geol. Mineral, Vietnam. Hanoi 154 pp.

Cai, Y., Wang, Y., Cawood, P.A., Zhang, Y., Zhang, A., 2015. Neoproterozoic crustal growth of the Southern Yangtze Block: Geochemical and zircon U-Pb geochronological and Lu-Hf isotopic evidence of Neoproterozoic diorite from the Ailaoshan zone. Precambr. Res. 266, 137–149.

Cai, Y.F., Wang, Y.J., Cawood, P.A., Fan, W.M., Liu, H.C., Xing, X.W., Zhang, Y.Z., 2014. Neoproterozoic subduction along the Ailaoshan zone, South China: geochronological and geochemical evidence from amphibolite. Precambr. Res. 245, 13–28.

Chau, N.D., Jadwiga, P., Adam, P., Duong, V.H., Phon, L.K., Paweł, J., 2017. General characteristics of rare earth and radioactive elements in Dong Pao deposit, Lai Chau, Vietnam. Vietnam J. Earth Sci. 39 (1), 14–26.

Chau, N.D., Le, K.P., Jodłowski, P., Pieczonka, J., Piestrzyński, A., Duong, V.H., Nowak, J., 2016. Natural Radioactivity at the Sin Quyen iron oxide copper gold deposit in North Vietnam. Acta Geophys. 64, 2305–2321.

Chen, H.Y., 2013. External sulphur in IOCG mineralization: implications on definition and classification of the IOCG clan. Ore Geol. Rev. 51, 74–78.

Chung, S.L., Lee, T.Y., Lo, C.H., Wang, P.L., Chen, C.Y., Yem, N.T., Hoa, T.T., Wu, G.Y., 1997. Intraplate extension prior to continental extrusion along the Ailao Shan Red River shear zone. Geology 25 (4), 311–314.
Cliff, R.A., 1985. Isotopic dating in metamorphic belts. J. Geol. Soc., London 97–110.
Corrigan, J., 1991. Inversion of apatite fission track data for thermal history information. J. Geophys. Res. 96, 21 927–21 941.
Dac, N.X., Zhao, X.F., HaiT, T., Deng, X.D., Li, J.W. 2020. Two episodes of REEs mineralization at the Sin Quyen IOCG deposit, NW Vietnam. Ore Geol. Rev., 125, https://doi.org/10.1016/j.oregeorev.2020.103676.
Deng, J., Wang, Q.F., Li, G.J., Hou, Z.Q., Jiang, C.Z., Danyushevsky, L., 2015. Geology and genesis of the giant Beiya porphyry-skarn gold deposit, northwestern Yangtze Block, China. Ore Geol. Rev. 70, 457–485.
Dodson, M.H, 1973. Closure temperature in cooling geochronological and petrological systems. Contrib. Mineral. Petrol. 40, 259–274.
Duan, B.V., Duong, N.A., 2017. The relation between fault movement potential and seismic activity of major faults in Northwestern Vietnam. Vietnam J. Earth Sci. 39 (3), 240–255.
ESCAP, 1990. Report of Economic and Social Commission for Asia and the Pacific, 1990.
Faure, M.M., Claude Lepvrier, C., Vuong Van Nguyen, V.V., Tich Van Vu, T.V., Wei Lin, V., Zechao Chen, Z, 2014. The South China block-Indochina collision: Where, when, and how. J. Asian Earth Sci. 79 (2014) 260–274.
Findlay, R.H., 2018. Geometry, kinematics and regional significance of faulting and related lamprophyric intrusion in the mineralized zone at the Pu Sam Cap complex, Northwest Vietnam. Vietnam J. Earth Sci. 40 (4), 320–340.
Findlay, R.H., Trinh, P.T., 1997. The structural setting of Song Ma region, Vietnam and the Indochina-South China plate boundary problem. Gondwana Res. 1 (1), 11–33.
Frimmel, H.E., 2008. Earth's continental crustal gold endowment. Earth Planet. Sci. Lett. 267, 45–55.
Garnier, G.G., Maluski, H., Ohnenstetter, D., Trinh, P.T., Hoàng, Q.V., Pham, V.L., Vu, V. T., Schwarz, D., 2002. Ar-Ar ages in phlogopites from marble-hosted ruby deposits in northern Vietnam: evidence for Cenozoic ruby formation. Chem. Geol. 188, 33–49.
Garnier, V., Ohnenstetter, D., Giuliani, G., Maluski, H., Deloule, E., Trinh, P.T., Long, P. V., Vinh, H.Q., 2005. Age and significance of ruby-bearing marble from the Red reiver shear zone, Northern Vietnam. Can. Mineral. 43, 1315–1329.
Garnier, V., Giuliani, G., Ohnenstetter, D., Fallick, A.E., Dubessy, J., Banks, D., Vinh, H. Q., Lhomme, Th., Maluski, H., Pêcher, A., Bakhsh, K.A., Long, P.V., Trinh, P.T., Schwarz, D., 2008. Marble-hosted ruby deposits from Central and Southeast Asia: Towards a new genetic model. Ore Geol. Rev. 34, 169–191.
Gaskov, I.V., Tran, T.A., Tran, T.H., Pham, T.D., Nevolko, P.A., Pham, N.C., 2012. The Sin Quyen Cu-Fe-Au-REE deposit (northern Vietnam) composition and formation conditions. Russ. Geol. Geophys. 53, 442–456.
Gilley, L.D., Harrison, T.M., Leloup, P.H., Ryerson, F.J., Lovera, O.M., Wang, J.H., 2003. Direct dating of left-lateral deformation along the Red River shear zone, China, Vietnam. J. Geophys. Res. 108 https://doi.org/10.1029/2001JB0011726.
Giuliani, G., Dubessy, J., Banks, D., Hoang Quang V., Lhomme, T.H., Pironon, J., Garnier, V., Trinh, P.T., Pham Van, L., 2003. Ohnenstetter D., D. Schwarz., 2003. Co2-H2S-COS-ALO(OH) bearing fluid inclusions in ruby from marble-hosted deposits in Luc Yen area , North Vietnam, Chem. Geol.194, 167-185.
Giuliani, G., Hoang Quang, V., Trinh, P.T., France-Lanord, Ch., Coget, P., 1999. Carbon isoptopes study on graphite and coexisting calcite-graphite pairs in marbles from the Luc Yen and Yen Bai districts, North of Vietnam. Bull. Liaison SFMC 11, 80–82.
Green, P.F., Duddy, I.R., Laslett, G.M., Hegarty, K.A., Glea dow, A.J.W., Lowering, J.F., 1989. Thermal annealing of fission tracks in apatite, 4. Quantitative modelling techniques and extension to geological timescales. Chem. Geol. 79, 155–182.
Hao, D.V., 2018PhD Dissertation: Rare earth, natural radionuclides and selected precious metals in the iron oxides, copper and gold (IOCG) Sin Quyen deposit, Lao Cai, North Vietnam. 2018, AGH UST, Krakow, Poland.
Hames, W.E, Bowring, S.A, 1994. An empirical evaluation ofthe argon diVusion geometry in muscovite. Earth Planet. Sci. Lett. 124, 161–167.
Harrison, T.M, Armstrong, R.L., Clarke, G.K.C., 1978. Thermal models and cooling histories from fission-track, K–Ar, Rb/Sr and U/Pb mineral dates, Northern Coast Pluton Complex British Colombia abstract. In: Short Papers of the Fourth International Conference on Geochronology, Cosmochronology, Isotope Geology. U. S. Geol. Surv 167–170.
Harrison, T.M, Armstrong, R.L., Naeser, C.W., Harakal, J.E., 1979. Geochronology and thermal history of the coast plutonic complex, near Prince Rupert, British Columbia. Can. J. Earth Sci. 16, 400–410.
Harrison, T.M., Leloup, P.H., Ryerson, F.J., Tapponnier, P., Lacassin, R., Chen, W., 1996. Diachronous initiation of transtension along the Ailao Shan-Red River shear zone, Yunnan and Vietnam. World Reg. Geol. 208–226.
He, W.Y., Mo, X.X., He, Z.H., White, N.C., Chen, J.B., Yang, K.H., Wang, R., Yu, X.H., Dong, G.C., Huang, X.F., 2015. The geology and mineralogy of the beiya skarn gold deposit in Yunnan, southwest China. Econ. Geol. 110, 1625–1641.
Hieu, P.T., Chen, F.K., Thuy, N.T.B., Nguyen, Q.C., Li, S.Q., 2013. Geochemistry and zircon U-Pb and Hf isotopic composition of Permian alkali granitoids of the Phan Si Pan zone in northwestern Vietnam. J. Geodyn. 69, 106–121.
Hitzman, M.W., 2000. Iron oxide-Cu-Au deposits: what, where, when, and why. In: Porter, T.M. (Ed.), Hydrothermal iron oxide copper–gold & related deposits: a global perspective. PGC, Adelaide, pp. 9–25.
Hitzman, M.W., Oreskes, N., Einaudi, M.T., 1992. Geological characteristics and tectonic setting of Proterozoic iron oxide (Cu–U–Au-REE) deposit. Precambr. Res. 58, 241–287.
Hitzman, M.W., Valenta, R.K., 2005. Uranium in iron oxide-copper–gold (IOCG) systems. Econ. Geol. 100, 1657–1661.
Hsin, H.H., Zhen, J.X., Yih, M.W., Xiaodong, S., Bor, S.H., Le, M.N., 2013. First local seismic tomography for Red River shear zone, northern Vietnam: Stepwise inversion employing crustal P and Pn waves. Tectonophysics 584, 230–239.
Hu, X.Z., Huang, Z., 1997. The petrology and petrogensis of the Yangtze plantfrom western margins alkali-rich granite porphyry. Geotecton. Metall. 21, 173–180 (in Chinese with English abstract).
Hu, Y.Z., Tang, S.H., Wang, H.P., Yang, Y.Q., Deng, J., 1995. Geology of the Ailaoshan Gold Deposits. Geological Publishing House, Beijing.
Hu, Z.C., Zhang, W., Liu, Y.S., Gao, S., Li, M., Zong, K.Q., Chen, H.H., Hu, S.H., 2015. "Wave" signal-smoothing and mercury-removing device for laser ablation quadrupole and multiple collector ICPMS analysis: application to lead isotope analysis. Anal. Chem. 87 (2), 1152–1157.
Huong, L.T.T., Haeger, T., Phan, T.L., 2018. Study of impurity in blue spinel from the Luc Yen mining area, Yen Bai province, Vietnam. Vietnam J. Earth Sci. 40 (1), 47–55.
Huong, N.V., Phong, T.V., Trinh, P.T., Liem, N.V., Thanh, B.N., Pham, B.T., 2020. Recent tectonics, geodynamics and seismotectonics in the Ninh Thuan Nuclear Power plants and surrounding regions, South Vietnam. J. Asian Earth Sci. 187, 104080.
Hurford, A.J., 1986. Cooling and uplift patterns in the Lepon tine Alps South Central Switzerland and age of vertical movement on the Insubric fault line. Contrib. Mineral. Petrol. 92, 413–427.
Ishihara, S., Hideo, H., Mihoko, H., Pham, N.C., Pham, T.D., Tran, T.A., 2011. Mineralogical and chemical characteristics of the allanite-rich copper and iron ores from the Sin Quyen mine, northern Vietnam. Bull. Geol. Surv. Japan. 62 (5/6), 197–209.
Jacqueline, A., Halpin, Hai, T.T., Chun, K.L., Sebastien, M., Anthon, J., Crawford, Khin, Z., 2016. U-Pb zircon geochronology and geochemistry from NE Vietnam: A 'tectonically disputed' territory between the Indochina and South China blocks. Gondwana Res. 34, 254–273.
Jian, X.C., Kai, Jun.Z., 2009. A new model for the Indochina and South China collision during the Late Permian to the Middle Triassic. J. Tectonophysics 467, 35–43.
Kazuhiro, T., Nadir, H., Yo-ichiro, O., Tran, V.T., Le, V.D., Shigeki, H., 2005. New paleomagnetic constraints on the extrusion of Indochina: Late Cretaceous results from the Song Da terrane, northern Vietnam. Earth Planet. Sci. Lett. 229 (3–4), 273–285.
Kerrich, R., Goldfarb, R., Groves, D.I., Garwin, S., 2000. The geodynamics of world-class gold deposits: characteristics, space–time distribution, and origins. Rev. Econ. Geol. 13, 501–551.
Krenn, K., Huong, L.T.T., 2019. Fluid characteristics from shallow magmatic environments: A contribution to danburite bearing Luc Yen pegmatites, northern Vietnam. Vietnam. J. Earth Sci. 41 (1), 41 (1), 1–9.
Krismer, M., Vavtar, F., Ttropper, P., Sartory, B.K., Bernhard, Kaindal R., 2011-. Mineralogy, mineral chemistry and petrology of the Ag-bearing Cu-Fe-Pb-Zn sulphide mineralizations of the Pfunderere Berg (South Tyrol, Italy). Australian. J. Earth Sci. 104 (1), 36–48.
Le, D.B., Ngo, G.T., 1995. Phanerozoic Ophiolites in Indochina. Vietnam Journal of Geology, Special Issue, Proceedings of the International Symposium on the Geology of South East Asia and Adjacent Areas 5–6, 212–221.
Le, K.P., Nguyen, T.S., Tran, T.N., Lai, M.G., Piestrzynski, A., Pieczonka, J., Jodlowski, P., Nguyen, D.C., Nguyen, V.L., Nguyen, V.N., Do, T.H.T., 2015. Researching the procedures for survey and assessment of the radioactive environmental impacts due to mining and processing ores at the Sing Quyen cooper mine, Lao Cai province. In: 2-nd Inter. Conf. on Scien. Res. Cooperation between Vietnam and Poland in Earth Sciences. 4-6. pp. 359-369.
Lee, J.K.W., Williams, I.S., Ellis, D.J., 1997. Pb, U and Th diVusion in natural zircon. Nature 390, 159–161.
Leiluo, X., Xianwu, Bi, Ruizhong, H., Youqiang, Q., Yongyong, T., Xinsong, W., Jingjing, Z., 2016. Redox states and genesis of magmas associated with intra-continental porphyry Cu–Au mineralization within the Jinshajiang-Red River alkaline igneous belt, SW China. Ore Geol. Rev. 73, 330–345.
Leloup, P.H., Arnaud, N., Lacassin, R., Kienast, J.R., Harrison, T.M., Trinh, P.T., Replumaz, A., Tapponnier, P., 2001. New constraints on the structure, thermochronology, and timing of the Ailao Shan-Red River shear zone, AE Asia. J. Geophy. Res. 106 (B4), 6683–6732.
Leloup, P.H., Lacassin, R., Tapponnier, P., Scharer, U., Dalai, Zhong, Xiaohan, Liu, Liangshang, Zhang, Shaocheng, Ji, Trinh, P.T., 1995. The Ailao Shan-Red River shear zone (Yunnan, China), Tertiary transform boundary of Indochina. Tectonophysics 251, 3–84.
Lepvrier, C., Nguyen, V.V., Maluski, H., Phan, T.T., Van, V.T., 2008. Indosinian tectonics in Vietnam. C. R. Geosci. 340, 94–111.
Li, X.C., Zhou, M.E., Chen, W.T., Zhao, X.F., Tran, M.D., 2017. Uranium-lead dating of hydrothermal zircon and monazite from the Sin Quyen Fe-Cu-REE-Au-(U) deposit, northwesteren Vietnam. Miner Deposita.
Li, Z.C., Pei, X.Z., Li, R.B., Pei, L., Liu, C.J., Chen, Y.X., Xu, T., Yang, J., Wei, B., 2015. U-Pb Zircon Geochronology and Geochemistry of the Neoproterozoic Liujiaping Group Volcanics in the Northwest Margin of the Yangtze Block: Implications For the Breakup of the Rodinia Supercontinent. Acta Geol. Sin. (English Edition). 89 (4), 1213–1225.
Li, X.C., Zhou, M.F., 2018. The nature and origin of hydrothermal REE mineralization in the Sin Quyen deposit, northwestern Vietnam. Econ. Geol. 113 (3), 645–673.
Liang, H.Y., Campbell, I.H., Xie, Y.W., 2002. Zircon age dated by ELA-ICP-MS for ore bearing porphyry in Jinping Tongchang. Miner. Deposit 21 (Suppl.), 421–422.
Liem, N.V., Dat, N.P., Dieu, B.T., Phai, V.V., Trinh, P.T., Vinh, H.Q., 2016a. Assessment of geomorphic processes and active tectonics in con voi mountain range (northern Vietnam) using the hypsometric curve analysis method. Vietnam J. Earth Sci. 38 (2), 202–216.

Liem, N.V., Trinh, P.T., Vinh, H.Q., Huong, N.V., Quan, N.C., Phong, N.C., Dat, N.P., 2016b. Analyze the correlation between the geomorphic indices and recent tectonic active of the Lo River fault zone in southwest of Tam Dao range. Vietnam J. Earth Sci. 38 (1), 1–13.
Lien, N.T., Pho, N.V., 2018. Formation of secondary non-sulfide zinc ore in Cho Dien Pb-Zn deposits. Vietnam J. Earth Sci. 40 (3), 228–239.
Liu, J., Wang, A.J., Cao, S., Zou, Y.X., Tang, Y., Chen, Y., 2008a. Geochronology and tectonic implication of migmatites from Diancangshan, Western Yunnan, China. Acta Petrol. Sinica. 24 (3), 413–420 (in Chinese with English abstract).
Liu, J., Xiaoyu, C., Wenbin, W., Yuan, T., My, D.T., Quang, L.N., Zhaochong, Z., Zhidan, Z., 2015. New tectono-geochronological constraints on timing of shearing along the Ailao Shan-Red River shear zone: Implications for genesis of Ailao Shan gold mineralization. J. Asian Earth Sci. 103, 70–86.
Liu, J.L., Tang, Y., Tran, M.D., Cao, S., Zhao, L., Zhang, Z.C., Zhao, Z.D., Chen, W., 2012a. The nature of the Ailao Shan-Red River (ASRR) shear zone: Constraints from structural, microstructural and fabric analyses of metamorphic rocks from the Diancang Shan, Ailao Shan and Day Nui Con Voi massifs. J. Asian Earth Sci. 47, 231–251.
Liu, J.L., Tran, M.D., Tang, Y., Nguyen, Q.L., Tran, T.H., Wu, W.B., Chen, J.F., Zhang, Z. C., Zhao, Z.D., 2012b. Permo- Triassic granitoids in the northern part of the Truong Son belt, NW Vietnam: Geochronology, Geochemistry and tectonic implications. Gondwana Res. 22, 628–644.
Liu, Y.S., Gao, S., Hu, Z.C., Gao, C.G., Zong, K.Q., Wang, D.B., 2010. Continental and oceanic crust recycling-induced melt-peridotite interactions in the Trans-North China Orogen: U-Pb dating, Hf isotopes and trace elements in zircons of mantle xenoliths. J. Petrol. 51 (1–2), 537–571.
Liu, Y.S., Hu, Z.C., Gao, S., Günther, D., Xu, J., Gao, C.G., Chen, H.H., 2008b. In situ analysis of major and trace elements of anhydrous minerals by LA-ICP-MS without applying an internal standard. Chem. Geol. 257 (1–2), 34–43.
Liu, L., Chen, W.T., 2019. Geology, mineralization styles and age of ore-hosting rocks of the Proterozoic Longbohe-Sin Quyen Fe-Cu belt: Implications for regional metallogeny. Ore Geol. Rev. 111, 103013.
Long, P.V., Giuliani, G., Fallick, A.E., Boyce, A.J., Pardieu, V., 2018. Trace elements and oxygen isotopes of gem spinels in marble from the Luc Yen-An Phu areas, Yen Bai province, North Vietnam. Vietnam J. Earth Sci. 40 (2), 165–177.
Ludwig, K.R., 2003. ISOPLOT 3.00: A Geochronological Toolkit for Microsoft Excel. Berkeley Geochronology Center, California, Berkeley, p. 39.
Maluski, H., Lepvrier, C., Jolivet, L., Carter, A., Roques, D., Beyssac, O., Trong, T.T., Nguyen, D.T., Avigad, D., 2001. Ar–Ar and fission-track ages in the Song Chay Massif: early Triassic and Cenozoic tectonics in northern Vietnam. J. Asian Earth Sci. 19, 23–248.
McLean, R.N., 2001. The Sin Quyen iron oxide–copper–gold–rare earth oxide mineralisation of North Vietnam. In: Porter, T.M. (Ed.), Hydrothermal Iron Oxide and Copper-Gold Related Deposits: A Global Perspective, Vol. 2. PGC Publishing, Adelaide, pp. 293–301.
Metcalfe, I., 1995. Gondwana Dispersion and Asian Accretion. Vietnam Journal of Geology, Special Issue, Proceedings of the International Symposium on the Geology of South East Asia and Adjacent Areas 5–6, 223–266.
Mezger, K., 1990. Geochronology in granulites. In: Vielzeuf, D., Vidal, Ph. (Eds.), Granulites and Crustal Evolution. Kluwer, pp. 451–470.
Nguyen, Q.C., Tokarski, Antoni K., Swierczewska, Anna, Zuchiewiczc, Witold A., Yem, Nguyen Trong, 2013. Late Tertiary tectonics of the Red River Fault Zone: Structural evolution of sedimentary rocks. J. Geodyn. 69, 31–53.
Nguyen, V.L., Savichev, O.G., Domarenko, V.A., Tin, Q.D., 2017. Improved method for hydrochemical exploration of mineral resources. Vietnam J. Earth Sci. 39 (2), 167–180.
Nguyen, V.Y., Dung, P.T., Hoa, T.T., Anh, T.T., Hieu, P.T., 2019. Formation pressure-temperature (PT) of Ye Yen Sun granite. Vietnam J. Earth Sci 41 (2), 173–181.
Nhung, B.T., Phuong, N.H., Nam, N.T., 2017. Assessment of earthquake-induced ground liquefaction susceptibility for Hanoi city using geological and geomorphologic characteristics. Vietnam J. Earth Sci 39 (2), 139–154.
Nhung, B.T., Phuong, N.H., Nam, N.T., 2018. Assessment of earthquake-induced liquefaction hazard in urban areas of Hanoi city using LPI-based method. Vietnam J. Earth Sci 40 (1), 78–96.
Pham, N.C., Ishiyama, D., Tran, T.A., Sera, K., 2011. Mineralogical and geological characteristics of rare metals bearing Na Bop, Lung Hoai, Na Son and Sin Quyen base meta deposits Northern Vietnam. NMCC Annual Report 18, 49–55.
Pham, N.C., Tran, T.A., Tran, T.H., Vu, H.L., Pham, T.P.L., Ngo, T.H., 2020. Chemical compositions of amphiboles and their references to formation conditions of granitoids from Nam Rom and Song Ma massifs, Northwest Vietnam. Vietnam J. Earth Sci. 42 (1), 80–92.
Pham, T.H., Chen, F.K., Nguyen, T.B., Nguyen, Q.C., Li, S.H., 2013. Geochemistry and zircon U-Pb ages and Hf isotopic composition of Permian alkali granitoids of the Phan Si Pan zone in northwest Vietnam. J. Geodyn. 69, 106–121.
Pham, T.H., Chen, F.K., Wang, W., Tam, B.M., Nguyen, T.B.T., Hoa, T.X., Li, X.H., 2008. Formation ages of granites and metabasalts in the Song Ma belt of northwestern Vietnam and their tectonic implications. Conference Gondwana 13, Dali, China, Abstracts vol., 163.
Phuong, N.H., Truyen, P.T., Nam, N.T., 2018. Development of a Web-GIS based Decision Support System for earthquake warning service in Vietnam. Vietnam J. Earth Sci. 40 (3), 193–206.
Pidgeon, R.T., Aftalion, M., 1978. Cogenetic and inherited zircon U/Pb systems in granites: Paleozoic granites of Scotland and England. In: Bowes, D.R., Leake, B.E. (Eds.), Crustal Evolution in Northwestern Britain and Adjacent Regions, Geol. J. 10, 183–220.
Pieczonka J., Piestrzyński A., Chau N.D, Phon L. K., Jodłowski P. 2015- Rare Earth, radioactive and selected elements in the iron oxide copper gold Sin Quyen deposit in North Vietnam. In Viet-Pol 2015 second international conference on scientific research cooperation between Vietnam and Poland in Earth Sciences: 331-353.
Pieczonka, J., Chau, N.D., Piestrzyński, A., Phon, L.K., 2019. Timing of ore mineralization using ore mineralogy and U-Pb dating, Iron Oxide Copper Gold Sin Quyen deposit, North Vietnam. Geol. Q. 63 (4), 861–874.
Porter, T.M., 2010. Advances in the Understanding of IOCG and Related Deposits. In: Porter, T.M. (Ed.), Hydrothermal Iron Oxide Copper-Gold and Related Deposits: A Global Perspective V3. PGC Publishing, Adelaide, pp. 5–106.
Purdy, J.W, Jager, E, 1976. K–Ar Ages on Rockforming Minerals from the Central Alps. Mem. Ist. Geol. Mineral. Padova 31.
Qi, X.X., Zeng, L.S., Zhu, L.H., Hu, Z.C., Hou, K.J., 2012. Zircon U-Pb and Lu-Hf isotopic systematics of the Daping plutonic rocks: implications for the Neoproterozoic tectonic evolution of the northeastern margin of the Indochina block, Southwest China. Gondwana Res. 21, 180–193.
Roger, F., Leloup, P.H., Jolivet, L., Lacassin, R., Trinh, P.T., Brunel, M., Seward, D., 2000. Long and complex thermal history of the Song Chay metamorphic dome (northern Vietnam) by multi-system geochronology. Tectonophysics 321, 449–466.
Sillitoe, R.H., 2003. Iron oxide-copper–gold deposits: an Andean view. Mineral. Deposita 38, 787–812.
Sillitoe, R.H., 2012. Copper provinces. Society of Economic Geologists Special Publication 16, 1–18.
Skirrow, R.G., 2011. Controls on uranium in iron oxide copper–gold systems: insights from Proterozoic and Paleozoic deposits in southern Australia. In: Proceeding of the 11th Biennial SGA conference, pp. 482–484.
Sugaki, A., Kitakaze, A., Kojima, S., 1987-. Bulk composition ofintimate intergrowth of chalcopyrite and sphalerite and their genetic implications. Miner. Deposita 22, 26–32.
Sugaki, A., Kitakaze, A., Kojima, S., 1989-. Comment on the paper by Ch. Marignac: Sphalerite stars in chalcopyrite: Are they always the result of an unmixing process? Mineral. Deposita 24, 176–182.
Sun, X.M., Shi, G.Y., Xiong, D.X., Wang, S.W., Zai, W., Qu, W.J., Du, A.D., 2007. Platinum group elements geochemistry and Re–Os isotopic compositions of Daping gold deposit in Ailaoshan Gold Belt, Yunnan Province, China and their metallogenic implications. Acta Geol. Sinica 81, 394–404.
Ta, V. D et al., 1975. Report of geological surveys and their results performed at the IOCG Sin Quyen deposit in Lao Cai, North Vietnam. Main Department of Geology of Vietnam, 318 p. (in Vietnamese).
Tapponnier, P., Lacassin, R., Leloup, P.H., Schuarer, U., Zhong, D., Wu, H., Liu, X., Ji, S., Zhang, L., Zhong, J., 1990. The Ailao Shan/Red River metamorphic belt: Tertiary left-lateral shear between Indochina and South China. Nature 343, 431–437.
Thanh, N.T., Liu, P.J., Dong, M.D., Nhon, D.H., Dung, B.V., Phach, P.V., 2018. Late Pleistocene-Holocene sequence stratigraphy of the subaqueous Red River delta and the adjacent shelf. Vietnam J. Earth Sci. 40 (3), 271–288.
Thao, H.M., Hien, T.T., Anh, D.D., Nga, P.T., 2017. Mineralogical characteristics of graphite ore from Bao Ha deposit, Lao Cai Province and proposing a wise use. Vietnam J. Earth Sci. 39 (4), 324–336.
Tianjian, Y., Xiaoming, S., Guiyong, S., Dongsheng, L., Haoyang, Z., 2019. The genetic linkage between the Yuanjiang marble-hosted ruby deposit and Cenozoic tectonic evolution of the Ailao Shan-Red River shear zone (Southwest China). J. Asian Earth Sci. 177, 38–47.
Tong-Dzuy, T., Vu, K. (Eds.), 2011. Stratigraphic Units of Viet Nam, second ed. Vietnam National University Publisher, Hanoi, p. 554.
Tran, M.D., Junlai, L., Quang, L.N., Yue, C., Yuan, T., Zhijie, S., Zhaochong, Z., Zhidan, Z., 2014a. Cenozoic high-K alkaline magmatism and associated Cu–Mo–Au mineralization in the Jinping-Fan Si Pan region, southeastern Ailao Shan-Red River shear zone, southwestern China–northwestern Vietnam. J. Asian Earth Sci. 79, 858–872.
Tran, M.D., Liu, J.L., Nguyen, Q.L., Chen, Y., Tang, Y., Song, Z.J., Zhang, Z.C., Zhao, Z.D., 2014b. Cenozoic Cu–Mo–Au mineralization and associated high-K alkaline magmatism in the Jinping-Fan Si Pan region, southeastern Ailao Shan-Red River shear zone, southwestern China-northwestern Vietnam. J. Asian Earth Sci. 79, 858–872.
Tran, M.D., Liu, J., Li, X., Dang, M., 2016. Geology, Fluid inclusion and isotopic study of the Neoproterozoic Suoi Thau copper deposit, Northwest Vietnam. Acta Geol. Sin. (English edition) 90 (3), 913–927.
Tran, M.D., Liu, J., Nguyen, Q.L., Chen, Y., Tang, Yuan, 2010a. Zircon U-Pb ages and Hf isotopic composition of the Pu Sam Cap high-potassic alkaline rocks in northwest Vietnam and regional tectonic implication. Acta Petrol. Sin. 26 (6), 1902–1914 (in Chinese with English abstract).
Tran, M.D., Liu, J.L., Nguyen, Q.L., Chen, Y., Zou, Y.X., 2010b. Metallogenic epoch and metallic sources of O Quy Ho molybdenum deposit. Vietnam. Miner. Deposits 29, 371–378.
Tran, N.N., 2001. The Age of the Ca Vinh and Xom Giau complexes Dated by SHRIMP U-Pb Analysis of Zircon. Vietnam J. Geol. [in Vietnamese] 1–2, 1–10.
Tran, T.H., Hoang, N., 2018. Petrology, geochemistry, and Sr, Nd isotopes of mantle xenolith in Nghia Dan alkaline basalt (West Nghe An): implications for lithospheric mantle characteristics beneath the region. Vietnam J. Earth Sci. 40 (3), 207–227.
Tran, V.T., 1979. Geology of Vietnam [the North Part]. Science and Technology Publishing House, Hanoi, pp. 78–95.
Trinh, P.T., Vinh, H.Q., Huong, N.V., Liem, N.V., 2013. Active fault segmentation and seismic hazard in Hoa-Binh reservoir, Vietnam. Cent. Eur. J. Geosci. 5 (2), 223–235.
Trinh, P.T., Leloup, H., Lacassin, R., Arnau, N., 1998. Formation of Ruby in the Red River metamorphic zone. Proceedings NCST Vietnam 10 (1), 143–148.

Trinh, P.T., Yem, N.T., Leloup, H., Tapponnier, P., 1994. Cenozoic stress field in north Vietnam from microtectonic measurement. Proceeding "International wokshop on seismotectonics and seismic hazards in South East Asia". Hanoi. 182–186.
Trinh, P.T., Liem, N.V., Huong, N.V., Vinh, H.Q., Thom, B.V., Thao, B.T., Tan, M.T., Hoang, N., 2012. Late Quaternary tectonics and seismotectonics along the Red River fault zone, North Vietnam. Earth Sci. Rev. 114, 224–235.
Truyen, P.T., Phuong, N.H., 2019. Probabilistic seismic hazard assessment for Hanoi city. Vietnam J. Earth Sci. 41 (4), 321–338.
Usuki, T., Lan, C.Y., Hoa, Tran, Trong, T.H., Dung, Pham, Thi, T.D., Wang, K.L., Shellnutt, J.G., Chung, S.L., 2015. Zircon U-Pb ages and Hf isotopic compositions of alkaline silicic magmatic rocks in the Phan Si Pan–Tu Le region, northern Vietnam: Identification of a displaced western extension of the Emeishan Large Igneous Province. J. Asian Earth Sci. 97, 102–124.
Van, H.D., Dinh, C.N., Piestrzynski, A., Pieczonka, J. 2021. Relationship between some selected major, minor and trace elements in the IOCG deposits (on the example of the unique Sin Quyen deposit, Lao Cai province, north Vietnam). J. Russ. Geol. Geophys. (in proof).
Wang, D.H., 2005. Cenozoic Metallogeny in China. Geological Publishing House, Beijing, p. 853.
Wang, D.H., Qu, W.J., Li, Z.W., Ying, H.L., Chen, Y.C., 2005. Mineralization episode of porphyry copper deposits in the Jinshajiang-Red River mineralization belt: Re-Os dating. Sci. China 192–198.
Wang, J.H., Qi, L., Yin, A., Xie, G.H., 2001a. Emplacement age and PGE geochemistry of lamprophyres in the Laowangzhai gold deposit, Yunnan, SWChina. Sci. China(Series D) 44 (Suppl.), 146–154.
Wang, J.H., Yin, A., Harrison, T.M., Grove, M., Zhang, Y.Q., Xie, G.H., 2001b. A tectonic model for Cenozoic igneous activities in the eastern Indo-Asian collision zone. Earth Planet Sci. Lett. 188, 123–133.
Wang, P.L., Lo, C.H., Lan, C.Y., Chung, S.L., Lee, T.Y., Tran, N.N., Sano, Y., 2011. Thermochronology of the PoSen complex, northern Vietnam: implications for tectonic evolution in SE Asia. J. Asian Earth Sci. 40, 1044–1055.
Williams, P.J., Barton, M.D., Johnson, D.A., Fontbote, L., De Haller, A., Mark, G., Oliver, N.H.S., Marschik, R., 2005. Iron oxide copper-gold deposits: geology, space-time distribution and possible modes of origin. Economic Geology 100th aniversary volume, 371–405.
Xu, L.L., Bi, X.W., Hu, R.Z., Zhang, X.C., Su, W.C., Qu, W.J., Hu, Z.C., Tang, Y.Y., 2012. Relationships between porphyry Cu-Mo mineralization in the Jinshajiang-Red River metallogenic belt and tectonic activity: Constraints from zircon U-Pb and molybdenite Re-Os geochronology. Ore Geol. Rev. 2012 (48), 460–473.
Yuan, F., Jiang, S.Y., Liu, J., Zhang, S., Xiao, Z., Liu, G., Hu, X., 2019. Geochronology and geochemistry of uraninite and coffinite: Insights into ore-forming process in the pegmatite-hosted uraniferous province, north qinling, central China. Minerals 9 (9), 552.
Zelazniewicz, A., Tran, H.T., Larionov, A., 2013. The significance of geological and zircon age data derived from the wall rocks of the Ailaoshan-red River shear zone, NW Vietnam. J. Geodyn. 69, 122–139.
Zhang, H., Li, C.Y., Yang, X.Y., Sun, Y.L., Deng, J.H., Liang, H.Y., Wang, R.L., Wang, B.H., Wang, Y.X., Sun, W.D., 2014a. Shapinggou: the largest Climax-type porphyry Mo deposit in China. Int. Geol. Rev. 56, 313–331.
Zhang, J., Deng, J., Chen, H.Y., Yang, L.Q., David, C., Leonid, D., Gong, Q.J., 2014b. LA-ICP-MS trace element analysis of pyrite from the Chang'an gold deposit, Sanjiang region, China: Implication for ore-forming process. Gondwana Res. 26, 557–575.
Zhang, J., Deng, J., Li, S.H., Yan, N., Yang, L.Q., Ma, N., Wang, Q.F., Gong, Q.J., 2010. Petrological characteristics of magmatites and their relationship with gold mineralization in the Chang'an gold deposit in southern Ailaoshan metallogenic belt. Acta Petrol. Sin. 26, 1740–1750.
Zhang, R.Y., Lo, C.H., Chung, S.L., Grove, M., Omori, S., Iizuka, Y., Liou, J.G., Tri, T.V., 2013. Origin and tectonic implication of ophiolite and eclogite in the Song Ma suture zone between the South China and Indochina blocks. J. Metamorph. Geol. 31, 49–62.
Zhao, X.F., Zhou, M.F., 2011. Fe–Cu deposits in the Kangdian region, SW China: a Proterozoic IOCG (iron-oxide–copper–gold) metallogenic province. Miner Deposita 731–747.
Zhen, Y., Li-Qiang, Y., Wen-Yan, H., Xue, G., Xu-Dong, L., Xin-Shang, B., Yi-Guan, L., 2017. Control of magmatic oxidation state in intracontinental porphyry mineralization: A case from Cu (Mo–Au) deposits in the Jinshajiang-Red River metallogenic belt, SW China. Ore Geol. Rev. 90, 827–846.
Zhu, X.P., Mo, X.X., White, N.C., Zhang, B., Sun, M.X., Wang, S., Wang, S.X., Zhao, S.L., Yang, Y., 2013. Petrogenesis and metallogenic setting of the Habo porphyry Cu-(Mo-Au) deposit, Yunnan, China. J. Asian Earth Sci. 66, 188–203.
Zhu, X.P., Mo, X.X., White, N.C., Zhang, B., Sun, M.X., Wang, S.X., Zhao, S.L., Yang, Y., 2009. Geology and metallogenetic setting of the Habo Porphyry Cu (Mo-Au) deposit, Yunnan. Acta Geol. Sin. 83, 1916–1928 (in Chinese with English abstract).
Zong, K.Q., Klemd, R., Yuan, Y., He, Z.Y., Guo, J.L., Shi, X.L., Liu, Y.S., Hu, Z.C., Zhang, Z.M., 2017. The assembly of Rodinia: The correlation of early Neoproterozoic (ca. 900 Ma) high-grade metamorphism and continental arc formation in the southern Beishan Orogen, southern Central Asian Orogenic Belt (CAOB). Precambr. Res. 290, 32–48.